1

Freeze-Drying of Parenteral Drug Products and Vaccines

Geoff Smith

LyoMetrics, Centre for Advanced Process Analytical Technologies, School of Pharmacy, De Montfort University, The Gateway, Leicester LE1 9BH, UK

1.1 Introduction

A number of low-molecular-weight drugs (e.g. semisynthetic cephalosporins), many novel biologic drug products (which are based around the complexity of proteins), and some vaccines (such as those against rabies and coronavirus disease-2019 [COVID-19]) are insufficiently stable in the format of the aqueous solution, which is invariably required for the main routes of parenteral delivery, i.e. by intravenous (IV), intramuscular (IM), and subcutaneous (SC) injection. Many people are now all too aware of this issue, having witnessed the requirement for ultra-low-temperature storage and distribution of the first generation of COVID vaccines. These challenges have driven the development of strategies to improve active pharmaceutical ingredient (API) stability, including formulation with buffers to reduce rate of degradation, protein engineering to enhance molecular stability, and, where adequate liquid-state shelf life cannot be achieved, freeze-drying [1, 2].

With the rise of biologic drug therapy and with estimates in the literature varying from 30% to 50% [3–6] of biologic drugs and vaccines requiring freeze-drying for shelf-life purposes, it is clear that freeze-drying will remain an important manufacturing process for the foreseeable future. Recently, a process for stabilizing mRNA COVID vaccines was demonstrated in the scientific literature [7], which might reduce the reliance on the requirement for cold-chain storage and shipment.

For now, it is the conventional large-batch processing method that dominates the industrial landscape. However, with more recent innovative production systems—such as spin-freeze-drying of individual vials or spray freeze-drying followed by aseptic filling of vials [8]—the future might see the repurposing of this established method, with faster, smaller-scale processing, novel packaging/devices, and parallel processing of different drug formulations, under intensive process conditions, enabling the pharma industry to respond to the expected/dramatic increase in the demand for the personalized and injectable drugs markets [9].

1.2 Freeze-Drying—An Overview

Pharmaceutical freeze-drying is a low-temperature and low-pressure process for removing solvent (mainly water) from a drug product solution, thus avoiding the use of elevated temperatures that might otherwise degrade the drug substance. Only occasionally, smaller amounts of other solvents, such as ethanol and tert-butanol, are used as cosolvents to improve drug solubility (and, in the case of tert-butanol, accelerate the drying process). The freeze-drying process is usually undertaken in the final product container (which is invariably a sterilized glass vial), thereby avoiding the need to aseptically fill the dried powder. The intention is to produce a "cake" of dried material that maintains the stability of the API (i.e. drug substance) to deliver a product with a commercially acceptable shelf life.

The cake is expected to be highly porous with a large internal surface area so that it dissolves rapidly when water is reintroduced to the product. This propensity to dissolve rapidly is not just a function of the porosity of the cake, but also the inherent solubility of the drug substance and the formulation additives, and gives rise to the term *lyophile*, i.e. solvent "loving" for the description of the drug product. The synonym for freeze-drying is *lyophilization*, in which the suffix "–ation" means the action or process of doing something. In freeze-drying, the action is to transform the solution of the drug into a lyophile, which is a material that has a strong affinity for a solvent [10].

Scanning electron micrographs (SEM) illustrate the features of the porous matrix, that is the cake, that forms once the frozen water has been removed (Figure 1.1).

The pore structure will generally mirror the structure of the ice that was removed in the drying process (provided the process is executed in such a way that the solids fraction left behind on removal of the ice does not change its architecture through softening and collapse). It is this porosity (and the high surface-to-volume ratio of the solid fraction) that also facilitates the removal of that smaller fraction of water that had not crystallized into ice during the freezing stage. This water is often referred to as the "bound" water, a term which is taken to imply an intimate association with the various solutes that make up the solids fraction of the dosage form, rather than water that is fixed within the solids matrix, and hence cannot be removed (which is clearly not the case, as evidenced by the ease by which the "bound" water is removed by the process of desorption). The final moisture content of the dried material at the end of the lyophilization cycle (and over the shelf-life of the product) is one of the critical quality attributes (CQAs) of the product, alongside the time to reconstitute the solid on addition of water for injection (WFI) or some other suitable vehicle. The term CQA is defined in the International Conference for Harmonization (ICH) Q8(R2) tripartite guideline as "a physical, chemical, biological, or microbiological property or characteristic that should be within an appropriate limit, range, or distribution to ensure the desired product quality [12]. CQAs are generally associated with the drug substance, excipients, intermediates (in-process materials) and drug product." CQAs are typically those aspects affecting product purity and identity, strength, and stability; however, there are others that are specific to the delivery system, e.g. the

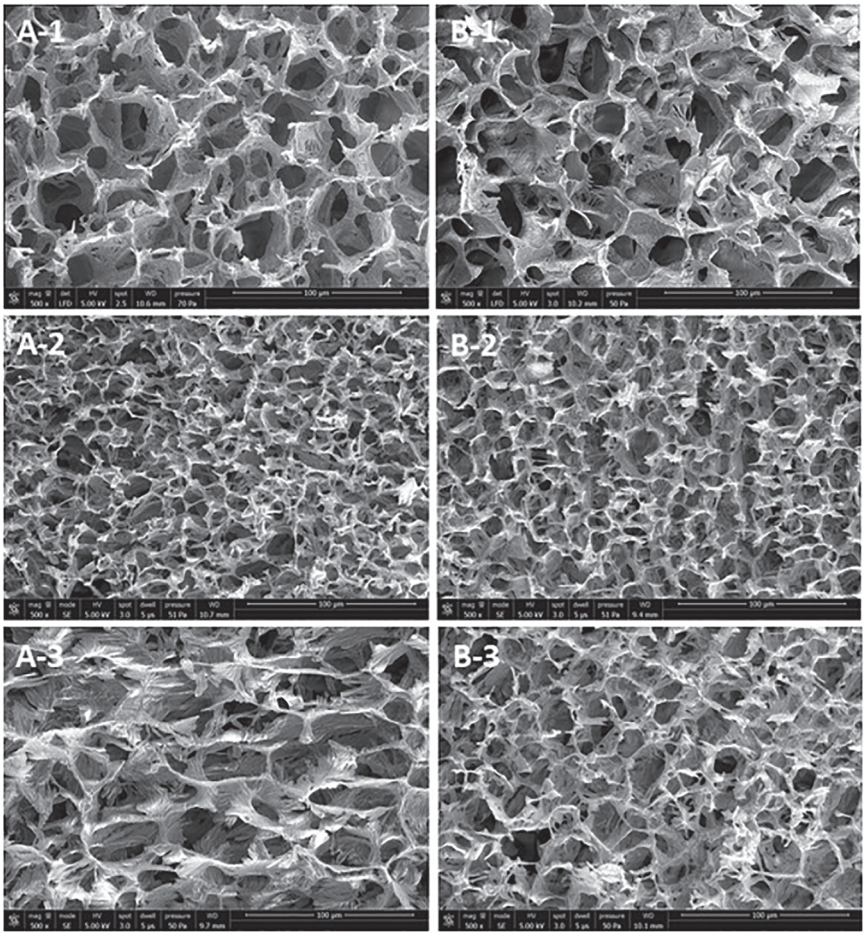

Figure 1.1 Scanning electron micrograph (SEM) of a lyo-cake structure *Source:* Badal Tejedor [11] / Elsevier / CC BY 4.0.

sterility of parenteral drug products and the drug release kinetics for implants. Table 1.1 gives a list of typical CQAs for a protein biopharmaceutical drug product.

The FDA's *Guide to Inspections of Lyophilization of Parenterals* [15] (see Figure 1.2) provides a useful summary of the process, which starts with the dissolution of the drug and excipients in WFI (other suitable cosolvents may be used), then passing the solution through a 0.22 μm pore size filter to remove microbes and particles before filling into sterile glass vials and partially stoppering the containers under aseptic conditions. The partially stoppered containers are loaded into the drying chamber of the freeze dryer, again under aseptic conditions. The solution is then frozen by cooling the shelves in the freeze-drying chamber or by prefreezing in another chamber before transferring to the dryer. The shelves may be pre-chilled in cases of low fill volume (where evaporation can occur before all the batch is loaded) or when the API is particularly unstable in solution. A vacuum is applied, and the shelves

Table 1.1 Critical quality attributes of a typical freeze-dried protein drug. Data from [13].

CQA	Requirements
Composition/strength/assay	Protein concentration, pH, excipient and buffer concentrations, osmolality, and extractable fill volume
Stability	Should be of sufficient level until the defined date of expiry
Purity and sterility	Level of contaminants (particulates, pyrogens, and adventitious agents[a)] should below a predefined limit of detection
Moisture content	The moisture content should be within predefined levels. Moisture can impact stability and shelf life
Visual appearance	Elegant-looking cake with a uniform cake appearance that does not show any observable signs of collapse/melt-back
Reconstitution time	Should completely dissolve within seconds to minutes

a) World Health Organization (WHO) guidance [14] defines an adventitious agent as any "contaminating microorganism of the cell culture or starting/raw materials (including bacteria, fungi, mycoplasmas/spiroplasmas, mycobacteria, rickettsia, protozoa, parasites, transmissible spongiform encephalopathies and viruses) that have been unintentionally introduced into the manufacturing process of a biological product. The source of the contaminant may be the legacy of the cell line, the raw materials used in the culture medium to propagate the cells (in banking, in production, or in their legacy), the environment, personnel, equipment, or elsewhere."

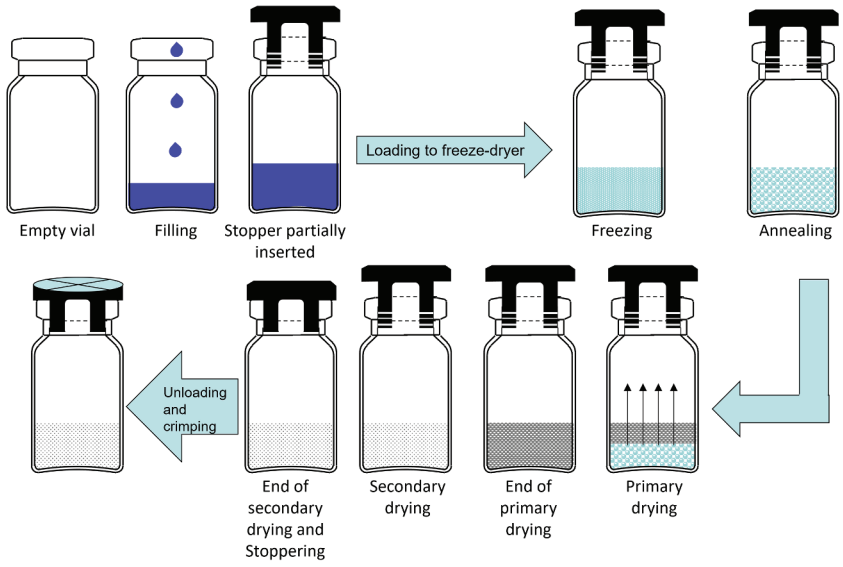

Figure 1.2 Schematic of the fill-finish process based on a lyophilization cycle.
Source: [1] / De Montfort University / CC BY 4.0.

are then heated to sublimate the ice from the frozen state (primary drying), before switching to the final drying stage to desorb water from the solids fraction (secondary drying). The stoppers are then fully inserted into the vials by a hydraulic stoppering mechanism that is built into the dryer.

1.3 Product Formulation

1.3.1 Understanding the Drug Substance

The drug development process starts with a preformulation programme aimed at understanding the physicochemical properties of the drug substance. The first requirement is to develop an analytical method (for example, a simple UV spectroscopic method) and to assess the stability of the drug to heat, light, and oxygen in the solid state, which is usually crystalline for small-molecule drugs. Next is an assessment of any impurities or solvents in the bulk drug substance that might carry through into the final drug product. The analytical method is used to determine the intrinsic solubility of the drug substance, including an assessment of the acid dissociation constant (pK_a) for small molecules or the isoelectric point (pI) for proteins, and whether the drug has intrinsic buffering capacity to maintain the solution at an optimal pH following the simple addition of either hydrochloric acid or sodium hydroxide.

Specific studies related to the development of the freeze-dried formulation then assess whether freezing of the drug solution yields a crystalline or an amorphous solids fraction (i.e. cake). These studies also determine the melting temperature and glass transition temperature of these phases, respectively, when the drug is freeze-dried alone. At this stage, it is necessary to consider whether the drug substance can be successfully freeze-dried without additives; if not, excipients should be introduced in a judicious and purpose-driven manner.

1.3.2 Excipients in Freeze-Dried Drug Product Development

Excipients are inactive substances that are combined with the drug substance to give what is known as the formulation (or, recipe, in more colloquial terms). The role of these agents is to enable a drug to be presented as a dosage form (i.e. the drug product) that can be manufactured routinely as a safe and efficacious product with an acceptible shelf life and convenient administration method. The formulation should therefore stabilize the drug substance and optimize its performance during manufacturing, storage, and reconstitution, which is the step whereby a vehicle, such as WFI, is reintroduced to the freeze-dried product to return it to its liquid form [16].

The general advice on the use of excipients [17–19] is to:

- Only introduce an excipient if it serves a purpose in the formulation.
- Check the compatibility with the active drug substance, i.e. the absence of undesired chemical or physical interaction.
- Explore a range of formulations that show good stability and to avoid narrowing the options too early in development.

Table 1.2 Example formulation of a monoclonal antibody, siltuximab.

Siltuximab	100	mg
L-histidine	3.7	mg
From L-histidine and L-histidine monohydrochloride monohydrate		
Polysorbate 80	0.8	mg
Sucrose	169	mg
Diluent		
Sterile Water for Injection, USP.	5.2	ml

Source: Adapted from ref. [22].

- Verify the grade (quality/purity) available and the reliability and flexibility of its supply chain so you do not run out during clinical studies.

Small drug molecules often require quite simple formulations, with some high-dose products (i.e. aqueous solution of drug in concentrations in the region 5–10%) requiring only the addition of an acid or base (or a buffer) in order to provide an optimal pH to stabilize the drug substance. The lower dose drugs ($<10.0\,mg\,ml^{-1}$; 1% w/v) might need additional solids to bulk out the drug into an acceptable cake [20]. In constrast, large drug molecules, such as biotherapeutic proteins, have more demanding requirements in terms of their stability during the process of manufacture, reconstitution, and administration, as they are susceptible to multiple degradation pathways [21]. An example of a commercial formulation of a monoclonal antibody (a large molecular weight drug) is given in Table 1.2.

Unlike with the formulation of liquid injectable drug products, the formulations of freeze-dried products must also take account of the glass transition temperature and/or eutectic temperature of specific excipients. Evaluation of excipient mixtures and the final formulation is therefore essential to determine the risk of structural collapse during drying. In practice, the aim is to design a formulation with a high collapse temperature to allow drying at higher temperatures, either by adding agents that increase the glass transition of the liquid formulation when frozen or by avoiding substances that lower the glass transition, such as sodium chloride.

From various reviews [23–26], the commonly used excipients are classified according to their functionality, with some having more than one purpose (Table 1.3).

1.4 Freeze Dryer Components

A typical freeze dryer (Figure 1.3) comprises three primary components [33]:

1) A drying chamber, in which temperature-controlled shelves (carrying a heat-transfer fluid, usually a silicon oil) are loaded with a batch of vials, allowing for the product temperature inside each vial to be manipulated during the process.
2) A vacuum pumping system, to reduce the chamber pressure from atmospheric pressure (1 atm at sea level = 101,325 Pa or ~1 bar) to a pressure, usually, in the

Table 1.3 Categories of excipients used in freeze-drying, with their function and some examples.

Category	Function	Examples
Acids and bases	(i) To adjust the PH to ensure optimal API stability (ii) Reduce irritation on injection	NaOH, HCl
Buffering agent		Sodium citrate, sodium phosphate, and histidine [27]
Bulking agent	To produce an acceptable cake in low-dose APIs	Monosaccharide: mannitol Amino-acid: glycine Monosaccharide: sorbitol Disaccharides: sucrose, trehalose (lactose and maltose) [28]
Complexing agent	To improve solubility and stability	Hydroxypropyl-β-cyclodextrin (HP-β-CD) complex of ibuprofen [20]
Cosolvent	To improve API solubility	PEG, tert-butanol, propylene glycol, and glycerin (glycerol) [29]
Stabilizer	Stabilizer for the API (e.g. lyoprotectants for water replacement; or cryoprotectant as glassy matrix former to reduce aggregation	Common cryoprotectant: polyhydric alcohol Lyoprotectants: disaccharides (sucrose, trehalose), polysaccharides (dextran), amino acids (histidine) [28, 30–32]
Surfactant	To aid wetting and reconstitution	Polysorbate 20 or 80 [31]
Tc modifier	To increase the glass transition and therefore collapse temperature to allow for high drying temperatures	Dextran, proteins, large-molecular-weight polyethylene glycol (PEG >1 kD) [31]
Tonicity modifier	To reduce irritation at injection site	Dextrose, sodium chloride, and glycerol [20]
Antioxidant	To stabilize against oxidative degradation	Methionine, niacinamide
Preservative	To maintain sterility mainly in multiple-dose vials	Benzyl alcohol (the preservative is not part of the lyophilized formulation but is a component of the bacteriostatic water for injection, if used as the diluent) [29]

range to 5 Pa (50–500 μbar). These pressures are well below the triple point of ice (611.657 Pa at 0.01 °C)[1], allowing sublimation to occur during the primary drying stage, when heat is applied to the vials, while also establishing the

1 The triple point is the combination of temperature and pressure at which all three phases of water exist (i.e. solid/ice, liquid and gas/vapour are in equilibrium). Note that the symbol θ is used for temperatures on the Celsius scale whereas the symbol T is reserved for temperature on the Kelvin scale.

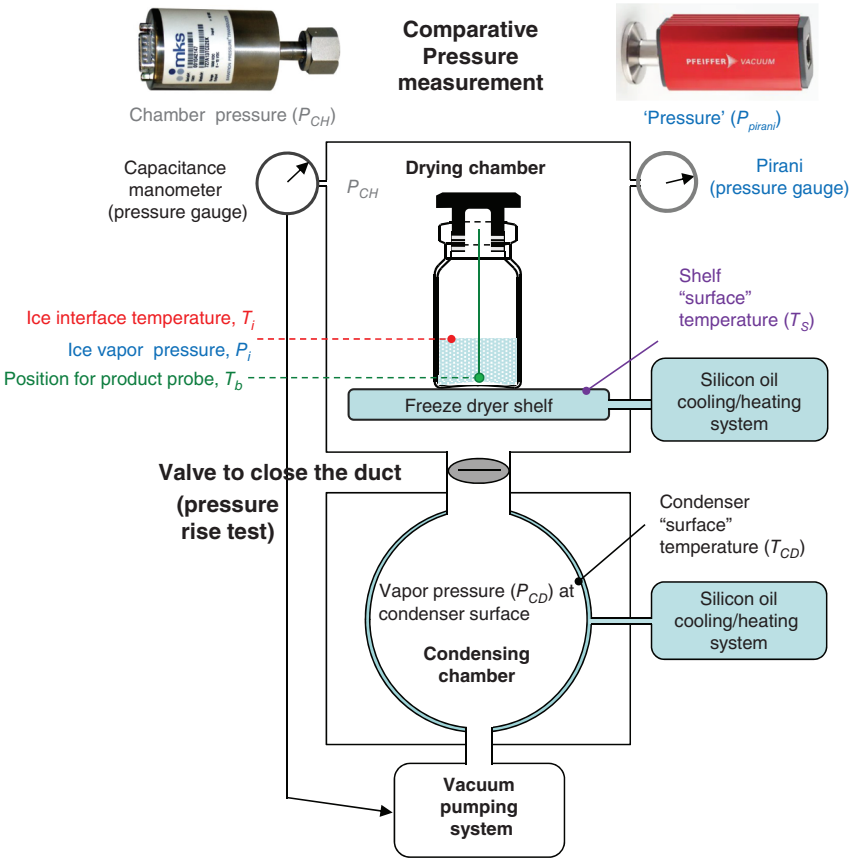

Figure 1.3 Simplified schematic of the typical components of a laboratory freeze dryer. Note (i) there will be multiple vials on the shelf, which are packed in a hexagonal arrangement, and (ii) the condensing chamber on intermediate to large dryers comprises a series of coils to increase the surface area for ice to condense. *Source:* [34] / Geoff Smith / CC BY 4.0.

diffusion gradient required for desorption of residual water during secondary drying.

3) A condensing chamber to capture/trap the water vapor evolved during both drying stages.

A typical large-scale industrial freeze dryer (Figure 1.4) can have ~40 m^2 of shelf area with 15 shelves, each of dimensions 1.5 m × 1.8 m with space for ~100,000 vials of nominal capacity 10 ml (outer diameter: 22 mm), and a controllable shelf temperature of −55 to +70 °C. One hundred thousand vials with an example fill volume of 2.5 ml and 5% w/v solids content would translate to a potential ice mass of ~235 kg. The condenser system of the dryer, therefore, requires careful design and considered engineering to ensure that it captures the ice before it has a chance of reaching the pumping system. The design and accessibility of its entire surface



Figure 1.4 Industrial scale freeze dryer. *Source:* Courtesy of GEA Lyophil.

area and maintenance of the condensing temperature of −75 °C are essential to the delivery of condenser capacities of 800–1000 kg/24 h ice. Such systems are also equipped with cleaning in place (CIP) and sterilization in place (SIP) capabilities, along with automatic loading (and unloading) systems to transfer the vials to the drying chamber from the filling line. Further details on the design of freeze dryers and their associated production plant may be found in Ref. [33].

1.4.1 The Vacuum System

Freeze-drying requires a vacuum, i.e. a reduction in the gas pressure within the drying chamber. In small, laboratory dryers, the set vacuum may be reached within 15 minutes whereas in the large commercial dryers, it may require tens of minutes (e.g. 20–30 minutes).

The acceptable pressure range for effective freeze-drying is, usually 50–500 μbar (5–50 Pa/37.5–375 mTorr). Given that much of the heat transfer between the shelves and the vials (required for ice sublimation) is dependent on conduction (and convection) through the gas within the chamber, pressures lower than 50 μbar (50 Pa/37.3 mTorr) are generally avoided. At such pressures, there are too few gas molecules to bring about effective heat transfer between the product and the shelf, resulting in slow drying. However, formulations with particularly low collapse temperatures ($Tc < -35$ °C) may require operation at lower pressures to minimise the risk of collapse during lyophilisation. See Ref. [35] for more information on vacuum technology, including the kinetic theory of gases, pressure and its measurement, and vacuum leaks.

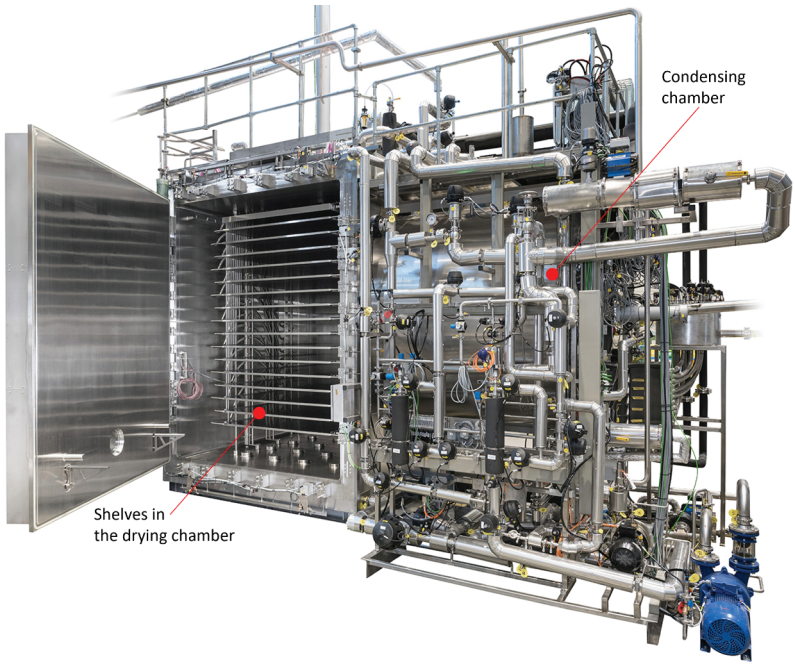

Figure 1.5 Front view of a large-scale industrial freeze dryer, showing the condensing chamber to the right of the drying chamber. The shelves in the drying chamber are in clear view but the condenser is largely obscured by the pipework. *Source:* Courtesy of GEA Lyophil.

1.4.2 The Condenser

Water molecules sublimed from the ice interface must be removed from the drying chamber to allow for more ice to sublime and to maintain the process of drying. This is achieved in most modern freeze dryers by a condenser located in a separate chamber and connected to the drying chamber via a duct, as shown in the schematic in Figure 1.3. Here, the condenser sits below the drying chamber, with a valve in the duct shown. In the example of a real, industrial scale dryer (Figure 1.5) the condensing chamber is to the right of the drying chamber. The role of the condenser is to "capture" the majority of the vapor released from the product, so preventing it from reaching the vacuum pump. See Ref. [33] for more information on the design of the condenser.

By maintaining a very low condenser temperature, relative to the ice interface temperature, it is possible to set up a significant concentration gradient in water vapor that ensures the sublimation process can continue. The absence of such a gradient would result in a buildup of water vapor (a back pressure) in the drying chamber causing the product temperature to increase (risking collapse of the product if it rises above T_c). The recommendation is that the condenser temperature should be at least 20 °C lower than the product temperature and so if freeze-drying with a target product temperature of −35 °C, for example, then a temperature of −75 °C that

is achievable by most freeze dryer condensers is clearly sufficient. The lowest temperature achievable by the condenser will be in the range −50 to −90 °C, depending on the type of refrigerant used.

The condenser temperature alone is not the only issue; it is also the capacity of the condenser to capture the ice that comes off which is important. Provided that it can condense the ice at a faster rate than it is generated, the system should function effectively. Of equal importance is that the buildup of ice layer on the condenser surface is not too thick, otherwise the ice temperature will rise above that of the core condenser temperature and impact its condensing capacity, see Ref. [33]. These factors may be addressed by ensuring that the surface area of the condenser is sufficiently large, for example, with a design based on direct-expansion coils of pipework in which the refrigerant evaporation extracts heat from the condenser surface [2].

1.5 Standard Process Instrumentation

The schematic of the typical freeze-dryer components in Figure 1.3 also shows the basic instrumentation (sensors), i.e. the product probes and the pressure gauges, that are routinely employed on dryers from pilot scale to commercial scale dryers. A review of best practices for their use in freeze-drying is given in Ref. [36].

1.5.1 Product Probes

During lyophilization cycle development, temperature sensors are routinely placed in selected vials across the dryer to monitor product temperature. These sensors are commonly referred to by the generic term, product probes. The sensing tip is usually placed at the bottom of the liquid in the vial, and so may not provide an accurate measurement of the critical temperature of the ice interface, especially with higher fill volumes, where temperature gradients will inevitably exist across the ice mass in the axial direction of the vial [37].

Thermocouples (TCs) and resistance temperature devices (RTDs) have been used historically for this purpose. Both have the disadvantage that the wiring (from the sensor to the measurement circuit) provides additional heat to the product. More recently, the introduction of the Tempris® wireless sensor has significantly reduced the additional heat flow to the product [38]. However, the physical placement of these sensors in the product might alter the way in which the ice structures form and hence impact the dry layer resistance with potential consequences for the rate of drying. It is generally assumed that the sensor provides additional sites for ice nucleation, and so, although nucleation is considered to be a stochastic (random) process, it generally occurs at a higher temperature than in those vials without these invasive probes. Nucleation at higher temperatures results in fewer nuclei and hence the growth of fewer, but larger ice crystals.

Chapter 2 provides a fuller account of the use of temperature sensors in freeze-drying, including the principles of operation, calibration, positioning within the dryer and vials, and their application to process monitoring and control.

1.5.2 Pressure Gauges

There are two pressure gauges attached to the drying chamber: one is a capacitance manometer that is used to determine the absolute pressure in the dryer (as it is insensitive to the type of gas), and the other is a Pirani gauge that can be used to assess the end of primary drying (as it is sensitive to water vapor).

A capacitance manometer comprises a pressure-sensitive membrane that forms part of an electrical capacitance cell. The physical force from the collisions of gas molecules causes the membrane to distort and changes the electrical capacitance of the cell. The higher the pressure, the greater the distortion and the greater the change in electrical capacitance. Given that gas pressure is dependent on the number concentration of molecules and their temperature, and not the molecular weight of the molecules, the sensor provides a measurement of pressure, which is independent of the type of gas molecule.

Pirani gauges comprise an electrically heated metal filament as part of a bridge circuit that is configured to measure changes in the electrical resistance of the filament. The gauge detects gas concentrations based on the impact of the thermal conductivity of the gas on the temperature and therefore electrical resistance of the heated filament. At higher gas pressures, there is more heat conducted away from the sensor (owing to a greater number of molecular collisions), and so the temperature of the sensor provides a measurement of pressure (the higher the pressure, the lower the filament temperature). However, different gases (e.g. nitrogen vs. water vapor) have different thermal conductivities, and so the measurement (i.e. the output from the sensor) is sensitive to the composition of the gas. In other words, for any given pressure, the sensor will give a different reading ("pressure" measurement) for two different compositions of gas. This phenomenon is exploited for the approximate determination of the end of sublimative (primary) drying, through a comparison between the outputs from the capacitance manometer and the Pirani gauge [33].

Chapter 3 provides a fuller account of the use of pressure sensors and vapour pressure measurement in freeze-drying, including capacitance manometers, Pirani gauges, calibration methods, and their application to process monitoring and pressure control.

1.6 Operational Parameters

The controllable operating parameters of a freeze dryer (i.e. the equipment settings) are the shelf temperature, the chamber pressure, and the condenser temperature; and it is the "time profile" of these parameters that defines what is generally known as the "lyophilization cycle." A typical lyo-cycle comprises the three main stages: freezing (with an optional annealing stage), primary drying (to remove the ice), and secondary drying (to remove the moisture associated with the solid fraction). Figure 1.6 shows the set temperatures and pressures of an example freeze-drying cycle.

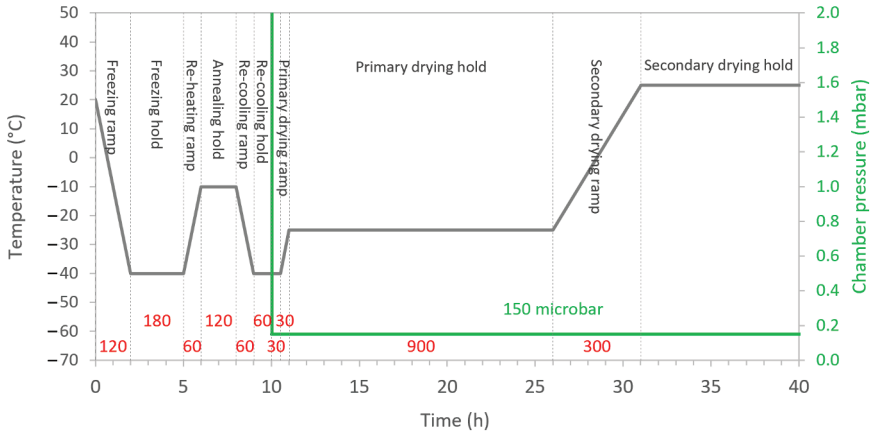

Figure 1.6 Example freeze-drying cycle showing the set values for the shelf temperature and the chamber pressure. The condenser temperature is not shown, but would typically be set to −75 °C before the application of the vacuum (green line). The numbers in red are the time periods in minutes for each step in the lyo cycle. *Source:* [39] / Geoff Smith / CC BY 4.0.

1.7 Process Parameters

The operator should know, or be able to predict, the process parameters that result from the interactions between the operating parameters, the equipment design, the product container, and the formulation attributes.

According to the ICH Q8(R2) Guideline on Pharmaceutical Development [12], the definition of a process parameter is one "whose variability has an impact on a critical quality attribute (CQA) and therefore should be monitored or controlled to ensure the process produces the desired quality." Ideally, a process parameter should be scale-independent and hence transferable between manufacturing scales.

There is a basic requirement that each stage of the process is completed before transitioning to the next stage: the solution should have frozen solid during the freezing stage before the vacuum is applied and the temperature ramped to initiate sublimation; all the ice must be removed from all vials before ramping the temperature further in the secondary drying stage; the target final moisture content must have been attained for all vials before applying the hydraulic ramp to collapse the shelves and stopper the vials. The primary drying time (i.e. the time taken to remove the ice from all vials) is one of the critical process parameters of a freeze-drying process.

For the majority of lyophilization processes, there is also a requirement for the ice interface temperature (during primary drying) and the dried layer temperature (during secondary drying) to remain below the collapse temperature and glass transition temperature respectively. This ensures preservation of an open network of pores to allow for the efflux of water vapor from ice sublimation and from desorption of water from the solid fraction. This can be expected to yield an end product with an acceptable moisture content (and hence shelf-life) which has an open pore structure and

hence redissolves completely within the target reconstitution time. The ice interface temperature is therefore another of the critical process parameters of the primary drying stage.

1.8 Designing the Freezing Stage

During the freezing stage, the free water within the solution (i.e. that which is not bound to the solutes) undergoes a change of state from liquid to solid (ice) (Figure 1.7). This occurs via four sequential steps [40].

1.8.1 Cooling Ramp and Process of Ice Formation

The first step of the freezing stage is supercooling of the liquid, i.e. the reduction of its temperature below the equilibrium melting point of ice. With the relatively slow cooling rates employed in a conventional freeze dryer (0.5–1 °C min^{-1}) in which vials are placed on temperature-controlled shelves, there is a global reduction in the

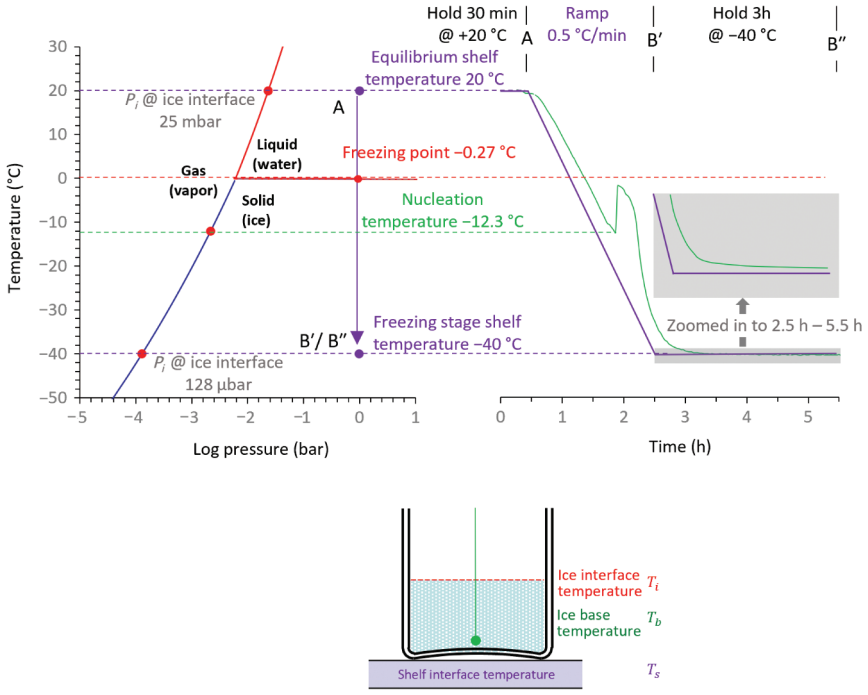

Figure 1.7 Example freezing profile for a 5% w/v sucrose solution, showing the shelf temperature (purple line) mapped onto the phase diagram of water (left side) and on the process log of the dryer (right side) with the product probe temperature (green line) recorded by a TC placed at the bottom of the vial. The initial equilibrium temperature is set at 20 °C, and the freezing temperature is set to −40 °C with a cooling rate of 0.5 °C min^{-1}. *Source:* [41] / Geoff Smith / CC BY 4.0.

temperature of the whole of the liquid, although there will be temperature gradients within individual vials and the bottom surface of the vial will inevitably be slightly colder than the top (and more so the greater the fill height of liquid within the vial).

The second step is the formation of ice nuclei. Commonly, in conventional cooling, ice starts to form at the vial bottom. In the process of controlled nucleation [42, 43] ice formation can occur from the top of the vials when there is an introduction of ice fog, or if nucleation is induced by pressurization, then de-pressurization of the chamber. Ice formation is an exothermic process that releases heat, which then immediately brings the temperature back from the supercooled state to just below the equilibrium melting temperature, which then arrests the formation of any more nuclei. Ice nuclei are more stable at low temperatures, and so it follows that the lower the nucleation temperature is, the greater the number of nuclei that will have formed.

There is then an immediate, spontaneous transition from nucleation to the third step, which is the ice growth phase whereby an ice front moves in the axial direction of the vial at a rate of a few millimeters per second, upwards in the case of conventional freezing and downwards in the case of controlled nucleation. Interestingly, the velocity of the ice front for any given solution increases with the degree of supercooling, presumably because there are more initial nuclei from which ice growth can proceed. However, the resulting ice crystals from low-temperature nucleation and faster growth will be generally smaller in size than those from the same solution that nucleates at the higher temperatures and experiences slower growth kinetics. This has important consequences for the subsequent primary drying stage, given that (i) the ice structure provides the initial template for the porosity of the dry layer that results once the ice fraction has been sublimed; (ii) the porosity is often pivotal in controlling the rate of diffusion of water vapor from the ice interface to the headspace of the vial. This rate-controlling feature of the dry layer is known as the dry layer resistance.

The fourth and final step follows on from the formation of ice and is due to the concentration of solutes that results as the solution is dehydrated. The concentration of certain bulking agents, such as mannitol and glycine, and buffers such as sodium citrate, might result in these solutes precipitating from solution. Concurrently, continued cooling of the non-ice fraction might also transform other parts of the unfrozen fraction into an amorphous glass (which is typical of the lyo-protectants such as sucrose). In the glassy state, this solute rich fraction (which is a mixture of the solutes and bound water) takes on the characteristics of a rigid, albeit brittle solid, whereas above the characteristic temperature at which the solute fraction transitions to the glassy state, this fraction takes on the characteristics of a viscous liquid and is susceptible to viscous flow resulting in a pronounced reduction in rigidity. Viscous flow might not be an issue when the ice crystals provide support for the interstitial spaces in the matrix, i.e. the solute fraction that occupies the spaces in between ice crystals. However, if viscous flow occurs as the ice fraction sublimes, then there is a high risk that the exposed, porous cake of solid will collapse.

1.8.2 Critical Temperatures

Before designing an effective freezing protocol, it is first essential to measure the critical parameters of the solution to be freeze-dried. These critical solution parameters are: the equilibrium melting point of the ice that forms from the freezing of the solution, the melting points of any crystalline solutes (often erroneously referred to as the eutectic temperature), the glass transition temperature of any amorphous phase, and the collapse temperature. For more information, see Ref. [2].

Apart from the collapse temperature, all these other temperatures may be obtained by subambient differential scanning calorimetry (DSC) or preferably by modulated differential scanning calorimetry (mDSC) [44]. Both methods employ two aluminum pans: one containing ~15–80 µl of the solution under test and the other empty (as a reference). The pans are simultaneously cooled to temperatures between −60 and −100 °C at a linear temperature ramp before reheating slowly back to ambient temperature. Modulated DSC differs from conventional DSC in that a sinusoidal modulation of temperature (of amplitude less than 0.5 °C) is overlaid on the linear temperature ramp.

Thermal transitions are observed from differences in heat flow to the sample pan and the reference pan as each is reheated. The temperatures at which any crystalline solute melts are observed by a spike in heat flow to the sample pan relative to the reference pan (which is required to supply the enthalpy of fusion). In contrast, the temperature at which the frozen solution passes through the glass-to-rubber transformation (known as the glass transition) is determined by a step change in the heat capacity of the rubbery/liquid state relative to the glassy/solid state.

Modulated DSC [45] allows the separation of the heat flow signal into two components: one that responds to the change in heating rate and one that does not. Generally, heat capacity-related events (such as the glass transition) respond to the change in heating rate, whereas kinetically driven events (such as reordering/recrystallization) do not. While standard DSC will show all the events being considered, modulated DSC investigations lend themselves nicely to lyophilization studies since there are, in effect, two heating rates being applied simultaneously to the sample. The underlying (average) heating rate can be slow to assist in the resolution of different transitions, and the instantaneous modulated heating rate can be set relatively high to improve the sensitivity to the glass transition.

An example of an mDSC cycle for the determination of the eutectic temperatures and/or glass transitions is given in Table 1.4.

A key feature of any DSC or mDSC protocol is the annealing step, which involves an increase in temperature from an initial ramp down to a low temperature (well below any anticipated glass transition) to a hold temperature below that at which ice melts, in order to increase the molecular diffusivity (mobility) of solutes. This is to (i) facilitate the growth of nuclei into a crystalline phase for those solutes with a natural propensity to crystallize, so that a melting endotherm can be observed in the second heating ramp, (ii) ensure the maximal volume of ice so that any measurement of a glass transition during the second heating ramp will be that of the maximally

Table 1.4 An example of an mDSC cycle for the determination of critical temperatures.

Step	Description
1	Cool to −70 °C at 10 °C min^{-1}
2	Hold for 15 min
3	Heat at 0.5 °C min^{-1} up to the annealing temperature (e.g. –10 °C)
4	Hold for 15 min
5	Cool to −70 °C at 10 °C min^{-1}
6	Hold for 15 min
7A	Start sine wave modulation with a 60-s cycle and an amplitude of ±0.5 °C
7B	Heat at 1.5 °C min^{-1} up to +25 °C while continually modulating the temperature

concentrated solute, which is given the specific symbol T_g' (pronounced "tee gee prime") [46].

The collapse temperature (T_c) is expected to be at least a few degrees higher than the glass transition (as so could be predicted by DSC methods). It is nevertheless good practice to determine its actual value using a freeze-drying microscope (FDM) because the difference between T_g' and T_c can in some cases be as high as 10 °C. With the FDM technique, the collapse of the dry layer is observed on a specialised cryo-microscope stage, one that not only cools and heats the sample but also allows for a vacuum to be applied to permit freeze-drying. During sublimation, the temperature of the stage is ramped slowly to force the product temperature to pass through the collapse temperature. The collapse event is then recorded from observations of the change in appearance of the drying front (i.e. that region just in front of the receding ice interface) based on the images that are acquired through the microscope lens (Figure 1.8). The dark/black areas are the dried region of the product where ice has been removed, leaving behind a porous layer that scatters, and therefore blocks the transmission of light. The mottled (birefringent, yellow/pink/purple) areas are the ice-rich regions of the frozen layer. Collapse is evident within the dried region from the appearance of gaps/holes through which light can now penetrate.

Photograph (a) taken at −35.0 °C shows a uniformly dark band, and hence dense dry layer structure. Photograph (b) taken at −34.0 °C shows that the structure is still maintained with no visible defects (voids) apparent. Photograph (c) taken at −33.0 °C shows that the structure at the drying front has just begun to stretch in places. Photograph (d) taken at −32.5 °C shows an increase in the size of the voids and confirms that the observation at −33.0 °C was indeed indicative of the onset of collapse and not due to a low, localized solute density. Photograph (e) taken at −32.0 °C shows that the loss of structure is much more apparent along much of the drying front. Photograph (f) taken at −31.5 °C shows that there is virtually no connectivity remaining between the frozen and dried material, and would be defined as total collapse.

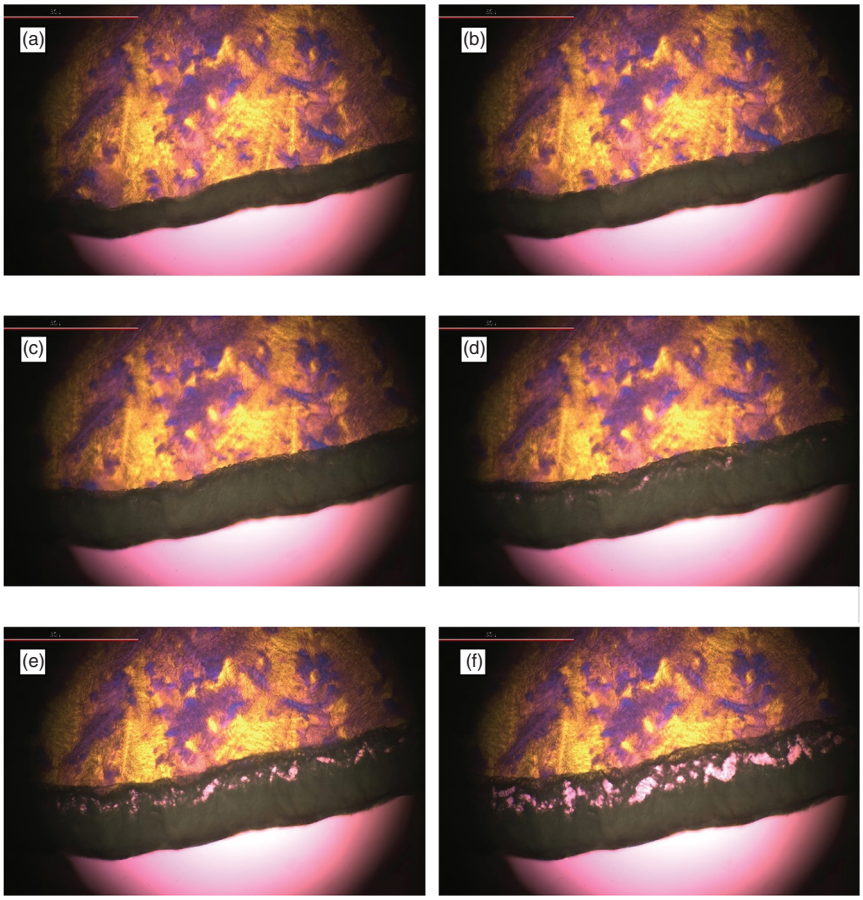

Figure 1.8 Freeze-drying microscope images for 4% sucrose solution recorded by a Biopharma Lyostat5. Further descriptions of each photograph are given in the text. *Source:* Courtesy of Biopharma Process Systems Ltd.

A point of concern with DSC and FDM observations of the thermal transitions relevant to the lyo cycle and formulation development (i.e. glass transition, devitrification, and solute melting) is that the sample size and thermal treatment of the solution differ from that within a freeze-drying vial. Consequently certain thermal characteristics might manifest differently in the actual freeze-drying process. In future, alternative methods such as through-vial impedance spectroscopy (TVIS), are likely to offer a more reliable characterization of actual in-vial thermal behavior [47].

1.8.3 Set Shelf Temperature

The product temperature is achieved by defining a target shelf temperature to be reached at the end of the cooling ramp (as one of the key operational parameters). This set temperature becomes a fixed parameter of the lyo cycle and therefore must accommodate differences in manufacturing environment, between the development stage activities and the commercial manufacturing processes. For example, a

drug product solution being investigated early in product development could easily have particles being introduced from a non-GMP environment; such particulates can act as nucleation sites and might only require −10 °C to initiate ice formation. Whereas sterile filtered solutions being filled into vials in a Class 1 environment will be particle free and hence contain fewer "seeds" for ice nucleation, and therefore might require temperatures as low as −30 °C to initiate ice formation.

The consideration of ice formation alone is insufficient when determining the set temperature of the shelf, as it must also be low enough to ensure that the product temperature goes below one or both of the following two critical temperatures:

1) The eutectic temperature of any crystalline-phase-forming excipients (e.g. glycine and mannitol) in a "first attempt" to crystallize those excipients.
2) The glass transition of any amorphous-phase-forming excipients to transform partial domains of noncrystalline phases (or the entirety of the unfrozen/solid fraction) into an amorphous glass.

Bearing in mind that the drug product solution is in a container made from glass (which has low thermal conductivity) while having a concave base and hence poor contact with the cooling source (the freeze dryer shelf), then the temperature of the drug product solution can be a few degrees Celsius higher than the set temperature of the shelf, especially in edge vials. This difference between the product temperature and the shelf temperature (ΔT) is impacted by two factors:

- The temperature of the shelf, with lower shelf temperatures increasing the value of ΔT, and
- The position of the vial on the shelf, with edge vials experiencing a higher ΔT because of the additional heat from side wall radiation.

Considering all factors together means that the set temperature for the shelf should be much lower than that required just for the ice crystallization (that was −30 °C in the above example) and invariably temperatures of −40 or even −50 °C are required.

1.8.4 Holding Period

In general, the heterogeneity of temperatures between all vials, coupled with the stochastic nature of ice crystallization and excipient crystallization, means that each vial has a unique time for it to reach thermal equilibrium with the shelf. To accommodate this inter-vial variation, there is inevitably a requirement for a holding period, at the set shelf temperature, to ensure that the contents of all vials are frozen solid before the next stage of ice sublimation is commenced. The term *frozen solid* means that the temperature has been reduced sufficiently not only to crystallize the ice but also to attempt to precipitate any solutes that might crystallize or at least to reduce the temperature below the glass transition temperature of those solutes that tend to form an amorphous phase. Without complete solidification, there is potential for the unfrozen fraction to collapse during primary drying, when the supporting ice structure has been removed.

At the end of the holding period, it might be expected for all vials to have reached thermal equilibrium. In other words, sufficient time must be allowed to reach the state whereby the latent heat of crystallization has been withdrawn from each vial, and the heat supplied to each vial is balanced by the heat flow from the vial (i.e. there is no net flow of heat in one direction or the other).

Note that *thermal equilibrium* does not necessarily mean that the content of every vial is in thermodynamic equilibrium (i.e. has the lowest energy state). Consider, for example, a vial that includes a crystallizing excipient such as mannitol, which is held at a temperature below its eutectic temperature, i.e. the temperature at which a saturated solution of the excipient should crystallize. The solution is in effect a supercooled liquid phase in which there is insufficient molecular mobility for the solute molecules to either self-assemble into the initial nuclei required for growth or for additional molecules to diffuse to the nuclei surface to grow the nuclei into crystalline particles (owing to the high viscosity of such solutions at these low temperatures). In thermodynamic terms, these systems are unstable or rather metastable, which means they have excess free energy but, given sufficient time (and catalyzed by any increase in temperature), can transform to the lower energy state of the crystalline form. For these metastable cases, an annealing stage may be required to promote crystallization.

1.8.5 Annealing

Annealing is a process, in which the shelf temperature and therefore frozen solution are reheated but not so high as to cross the phase boundary of water, thereby avoiding the ice melting.

The annealing stage serves two functions: The first is to promote the growth of larger ice crystals at the expense of smaller crystals (with the associated benefit of reducing the dry layer resistance and increasing the sublimation rate). This is known as Ostwald ripening. Given there is no net change in the amount of ice and therefore no change to the enthalpy of the system, this process cannot be observed on a differential thermal analysis trace. It is nevertheless a thermodynamically favorable process as it results in a lower free energy state because of the lower interfacial entropy associated with a lower surface to volume ratio of larger crystals relative to smaller crystals. The second is to ensure the crystallization of any solutes that have the thermodynamic propensity to do so (with the associated benefit of promoting the physical stability of the solid phase). The conversion of an amorphous, supercooled liquid state to a crystalline state is known as devitrification and is observed as an exothermic (heat-releasing) process on a differential thermal analysis trace. In this case, the formation of the new crystalline phase results in an exothermic peak in the DSC thermogram of heat flow.

1.9 Designing the Primary Drying Stage

In the primary drying stage, the ice fraction within the frozen solution is converted directly to the gaseous state (i.e. water vapor) by reducing the chamber pressure and

heating the shelves. This ensures the frozen solution reaches the phase boundary between solid (ice) and gas (vapor) and sublimation is initiated.

Having achieved the target temperature at the end of the freezing (and/or annealing stage), the first rule for attaining the target product temperature (T_p) in primary drying is that it must be maintained below the collapse temperature (T_c). Failure to do this can result in undesirable changes to the dry layer structure, resulting from viscous flow, which may lead to full or partial collapse of the pore structure (as stated previously). However, unlike the freezing stage where it is the shelf temperature that is controlled to achieve the target product temperature, in the primary drying stage, it is rather the chamber pressure (i.e. partial vacuum) that is used to indirectly control the product temperature.

In addition, as we shall see, it is a necessity that the shelf temperature (T_s) is higher than the product temperature (T_p) for there to be a temperature gradient across which heat can flow into the vial (to provide the latent heat of sublimation). Consequently, the shelf is often set to a temperature that is higher than the collapse temperature, while the product temperature (T_p) remains below the collapse temperature (T_c) as all the heat input is directed toward the sublimation of ice (latent heat) rather than being used to increase the temperature of the product (sensible heat).

An understanding of why it is the chamber pressure that effectively controls the product temperature may be approached by examining the phase diagram of water as a function of temperature and pressure (Figure 1.9). Although not directly related to freeze-drying, it is useful to consider what happens when water that was equilibrated at a room temperature of 20 °C and 1 bar (~1 atm) is heated to a temperature of 100 °C. This might be achieved by placing a beaker of water on an aluminum hot plate set to a temperature of 350 °C. The purple horizontal arrows in Figure 1.9 indicate the increase in temperature of the hot plate from 20 to 350 °C in separate studies at the three environmental pressures, with the top arrow indicating heating of the shelf at the first pressure of interest, i.e. 1 bar (10^5 Pa/750.062 Torr), and the bottom two arrows indicating that the shelf is heated while the environmental pressure is set to either 0.5 or 0.25 bar (which will be considered shortly).

At first, the heat input (referred to as the "sensible heat") is used to increase the temperature of the liquid from an initial 20 °C at which the vapor pressure above the liquid is 23 mbar (see the red dot at the corresponding temperature on the red line showing the phase boundary between the liquid and gaseous states of water). As the liquid heats up, there is an increase in the saturated vapor pressure at the surface of the liquid (as shown by the black arrow). The corresponding point on the phase boundary (again shown by another red dot) eventually coincides with the point on the purple line, indicating that the vapor pressure is now equal to the prevailing pressure of 1 bar once the product temperature reaches 100 °C.

Now that the saturated vapor pressure of water equals that of the environmental pressure, all the energy input thereafter is consumed in the evaporation of water. The liquid is then described as boiling as it transforms to the gas phase, i.e. vapor. During this change in state (otherwise known as a phase transition), the heat input is referred to as the "latent heat."

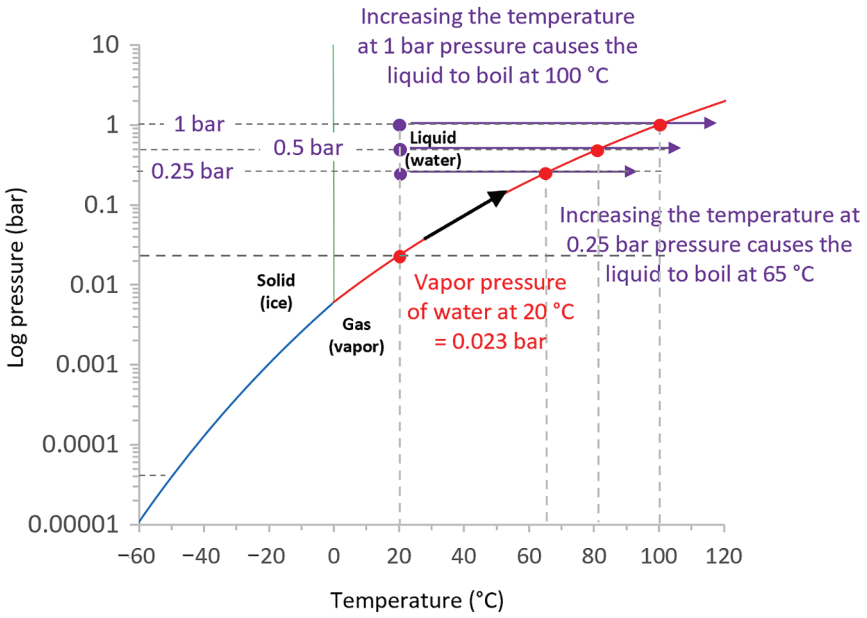

Figure 1.9 Phase diagram of water showing the phase boundaries between the solid, liquid, and gaseous states of water, with an illustration of how the boiling point changes from 65 to 81 °C and then 100 °C, as the prevailing experimental pressure is increased from 0.25 to 0.5 bar and then 1 bar. *Source:* [48] / Geoff Smith / CC BY 4.0.

Now, let us consider what happens if the water in the beaker on the hot plate is heated when the environmental pressure is either 0.5 or 0.25 bar, as indicated by the bottom two horizontal purple lines in Figure 1.9. From the phase diagram, it can be predicted that if the experiment were conducted under a partial vacuum of 0.5 bar (50,000 Pa), then the liquid would boil at the reduced temperature between 81 and 82 °C, whereas at 0.25 bar (25,000 Pa), the liquid would boil at a temperature between 65 and 66 °C, and so on. In such a manner, one can realize the possibility of indirectly controlling the boiling point by manipulation of the gas pressure.

The same principle applies to the sublimation of ice within a freeze dryer, whereby heat is supplied from the shelf to the vial to increase the temperature and hence vapor pressure at the ice interface, until it equals the prevailing pressure and the ice begins to sublime. However, before heat can be applied to transform the ice into water vapor it is first necessary to convert liquid water to ice. This is achieved by reducing the temperature below the freezing point of water (as was described in the previous section) and then reducing the pressure below the triple point of water, so that when the heat is input to the ice mass, that part of the frozen solid then transforms directly to the gaseous state, i.e. water vapor. These steps can be visualized by the sequence of purple lines in Figure 1.10. The first purple line from A to B shows the reduction in the shelf temperature required to freeze the liquid. Then the vertical line B to C shows the reduction in the chamber pressure (in this case to a new pressure of 300 μbar). Finally, line C to D shows the increase in shelf temperature which

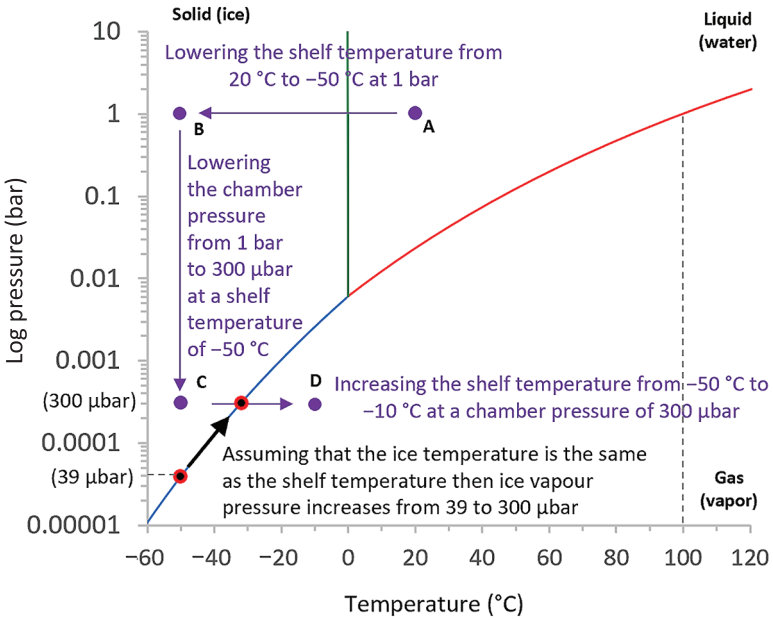

Figure 1.10 Phase diagram of water showing the phase boundaries between the solid, liquid, and gaseous states of water, with an illustration of how the freezing and ice sublimation occurs. The black arrow shows the increase in vapor pressure as the product temperature increases with the increase in shelf temperature. *Source:* [49] / Geoff Smith / CC BY 4.0.

increases the product temperature and hence vapor pressure at the surface of the ice. The increase in temperature of the product continues until the vapor pressure equals that of the chamber pressure, and thereafter all further heat input is consumed by the latent heat of ice sublimation, without any increase in temperature at the ice interface. Once again, the pressure in the chamber can be used to control the temperature at the ice interface during sublimation.

This control of the sublimation temperature of ice, via the chamber pressure, holds approximately true, at least during the initial stages of the sublimation of ice from a sample of pure water. However, there are essential differences between water boiling (evaporation) in an open beaker and ice sublimation from a vial, containing either pure ice or a frozen solution, that is placed on a shelf within a drying chamber, which is connected to a condensing chamber of a freeze dryer (Figure 1.3).

Provided that the beaker is left open to the atmosphere, the liquid will continue to boil without any increase in the prevailing pressure until all the liquid has evaporated. During this time, the boiling point remains constant at 100 °C. This is not quite so in the case of a freeze dryer. The condition that the vapor pressure at the ice interface equals that of the chamber only continues provided that there is a way to remove the vapor generated in the sublimation process (which is what the condenser is there for) and provided that the vent in the stopper and/or the dry layer

that develops on the removal of ice does not impede the transit of water molecules from the ice interface to the head space of the vial.

Without a condenser in the system, the removal of water vapor by the vacuum pump alone would not be able to keep pace with the rate of evolution of vapor from the sublimation of ice; or if the duct between the drying chamber and the condensing chamber was insufficient (i.e. too narrow) to cope with the rate of vapor generation, then with either scenario there would be an increase in the overall pressure within the drying chamber and a corresponding increase in the vapor pressure at the ice interface. These factors illustrate the constraints that a specific piece of equipment can place on the process of freeze-drying.

With regard to the product and its container (i.e. vial and stopper), the ideal condition of zero resistance to vapor flow from the ice interface to the drying chamber is not attainable in practice. Each constriction in the path of vapor flow from the ice interface to the chamber (which is already saturated with water vapor) contributes to the development of a back pressure, such that the vapor pressure at the ice interface (P_i) is higher than the vapor pressure in the head space of the vial due to the resistance to vapor flow provided by the channels in the solids fraction of the cake) and the vapor pressure (P_v) inside the head space of the vial is higher than inside the chamber (P_c) due to the restrictions created by the narrowing of the vial at its neck and the further restriction provided by the narrow opening created by the partially inserted stopper. The net result is that the vapor pressure at the ice interface, and therefore the ice interface temperature, increases above that one might predict from the set pressure in the drying chamber. These factors can be considered as some of the constraints that a specific product and its container place on the process of freeze-drying (the other being the collapse temperature, T_c). Each restriction that is placed on the free flow of water vapor is referred to as a resistance to vapor flow (Figure 1.11) and must be taken into account when designing the lyo cycle.

In all the above cases, the inevitable consequence of the increased ice interface pressure is an increase in the ice interface temperature, and an associated risk that the adjacent dry layer might exceed its collapse temperature.

Now let us turn our attention to what happens in an actual freeze-drying process by considering the "process log" of the freeze-drying cycle (Figure 1.12) for a solution of 15% IgG, formulated with 4% mannitol, 1% sucrose, 0.01% Tween 80, and 20-mM histidine. Note that the figure is based on real data but has been "stylized" (i.e. simplified) to demonstrate the various events that occur during primary drying. The lines on the trace are color coded as follows:

- Product temperatures are recorded by TCs placed at the bottom of selected vials (green line).
- Shelf temperature (T_s) is recorded as the inlet temperature of the thermal fluid entering the shelves (purple line).

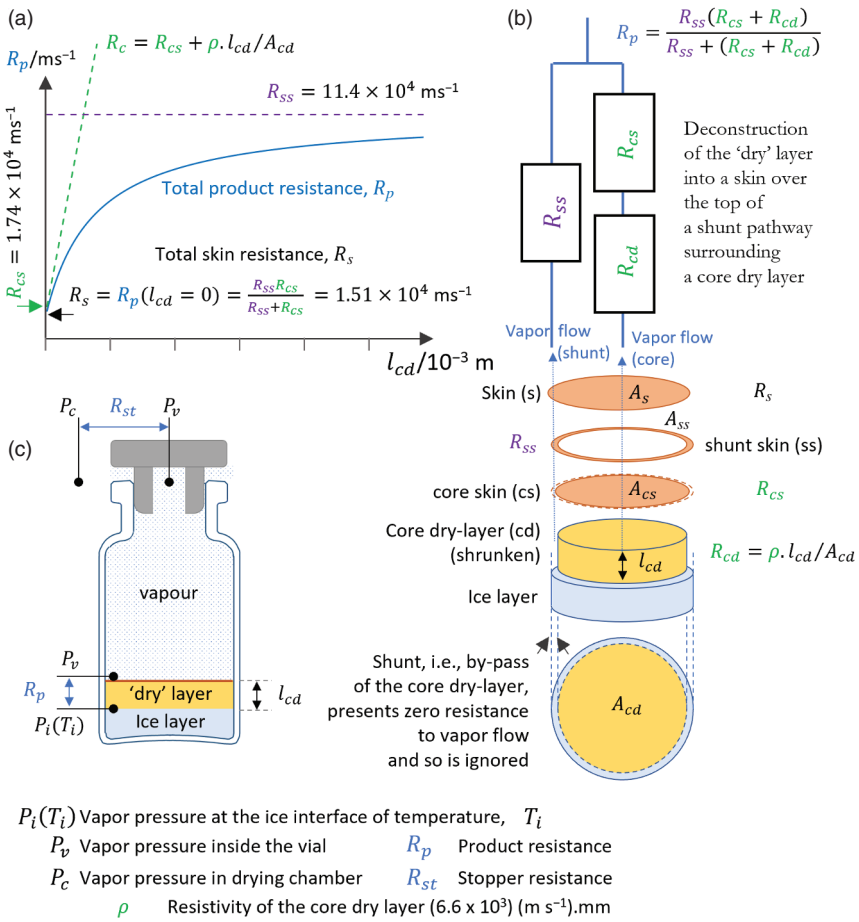

$P_i(T_i)$ Vapor pressure at the ice interface of temperature, T_i
P_v Vapor pressure inside the vial — R_p Product resistance
P_c Vapor pressure in drying chamber — R_{st} Stopper resistance
ρ Resistivity of the core dry layer (6.6 x 10^3) (m s^{-1}).mm

Figure 1.11 (a) A example profile for the increase in product resistance with the increased height of the dry layer, in which the dry layer has a skin layer on top and is partially shrunken from the walls of the vial. (b) A potential physical model for such a profile based on the product having a dry layer that extends across the entire internal diameter of the vial, below which there is a shrunken dry layer with a shunt pathway between the dry layer and the glass wall (note that the shunt pathway might be instead be due to cracks in the dry layer without shrinkage). (c) Illustration of the resistances to vapor flow associated with the narrowing pathways for vapor diffusion for the container and product. The first is associated with the vent in the stopper (R_s), and the second is associated with the connected pores within the dry layer (R_p). The transit of water vapor experiences these two resistances in sequence (i.e. one followed by the other), and hence it is possible to combine them into a single parameter $R_{ps,}$ which is the sum of R_p and R_s. *Source:* [50] / Geoff Smith / CC BY 4.0.

- Chamber pressure (P_c) is recorded by a capacitance manometer (gray line).
- A Pirani gauge, sensitive to the presence of water vapor, provides a method for determining the relative saturation of the chamber with water vapor (blue line).

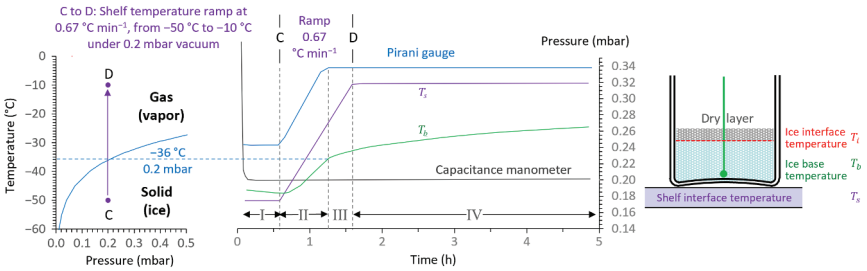

Figure 1.12 Example of sublimation of 15% IgG in vials placed at the core of the shelf (1% sucrose, 4% mannitol, 20 mM histidine, 0.01% Tween 20 as excipients). Primary drying was carried out at 0.2 mbar and −10 °C shelf temperature inside the Telstar Lyobeta freeze dryer. Note that each line is a stylized representation of real data to provide a more accessible picture of the expected trends one might observe in practice. *Source:* [51] / Geoff Smith / CC BY 4.0.

The process log has been annotated with the roman numerals I–V to indicate the various periods during which specific events may be observed during the primary drying stage.

(I) The first point to note is that, once the vacuum is applied, there is a small decrease in the product temperature (green line) due to a reduction in gas conduction at the lower pressures, which in turn reduces the heat supplied from the chamber.

(II) Next, soon after the shelf temperature starts to increase (purple line), the product temperature starts to increase, gradually at first and then more rapidly as the temperature difference between the shelf and vial increases. The lag between the rate of heating of the shelf and the rate of heating the vial inevitably results in an ever-increasing difference in the temperatures of the two objects. As the contents of the vial heat up, the increased temperature of the ice fraction results in an increased vapor pressure, and more vapor enters the chamber. This is picked up by the Pirani gauge (blue line). In fact, the pressure registered by the Pirani starts to increase as soon as there is an increase in the product temperature.

(III) At the point when the product temperature reaches −36 °C, the associated ice vapor pressure equals that of the chamber (0.2 mbar) and the ice starts to sublime and thereafter consumes all of the energy being received from the shelf. At this point, one would expect the temperature of the product to remain constant (due to the energy being used for the latent heat of sublimation as opposed to being used for sensible heat, to raise the temperature of the product). However, the fact that it continues to increase (albeit at a slower rate) is because of the development of a dry-layer resistance, which generates back pressure at the ice interface which then elevates the product temperature.

(IV) When the shelf temperature ramp finishes, the product temperature continues its ascent, again due to the ever-increasing dry layer resistance, as the height of the dry layer increases in size.

Note that during sublimation, the ice interface temperature will be colder than the temperature recorded at the base using the product probe.

In designing the cycle to allow for the creeping rise in the product temperature (once the shelf temperature ramp is complete), it might be necessary to introduce a safety margin of a lower shelf temperature to ensure that the ice interface temperature remains below the collapse temperature. Rather than relying on a trial-and-error approach, the freeze-drying community has devoted significant effort to creating process models and associated analytical instrumentation; these tools ensure that cycles may be transferred seamlessly between scales (from laboratory scale to commercial production). Scale-up is achieved by adjusting operational parameters, such as shelf temperature and chamber pressure, in response to ice interface temperature, heat transfer coefficient, and product dry layer resistance.

1.10 Designing the Secondary Drying Stage

At the end of primary drying, once the ice has sublimed, the solid fraction will have a moisture content in the region of 5–20%, depending on the moisture-binding capacity of the solids. In secondary drying, the shelf temperature is increased once more to provide the energy required to desorb moisture from the solids fraction, with typical shelf temperatures set to 20–50 °C at a ramp rate of 0.1–0.5 °C min^{-1} and a hold period of 4–12 hours Tang and Pikal [52].

A major concern, however, is that an excessive rate of increase in shelf temperature can drive the product temperature above the glass transition temperature, resulting in extensive shrinkage or even collapse. The glass transition temperature of the solids fraction is strongly dependent on moisture content, with residual moisture acting as a plasticizer that lowers the glass transition temperature. Consequently, if the shelf temperature is ramped too quickly before sufficient moisture has been desorbed, the product may exceed its moisture-dependent glass transition temperature, increasing the risk of collapse.

Another factor to consider is that during ice sublimation (primary drying), it is the connectivity and geometries of the pores left behind, once the ice is removed, that define the resistance to vapor flow. In secondary drying, however, it is instead the diffusion of moisture across the solid fraction that is the rate-limiting step, and hence the dry layer surface area becomes the rate-controlling step. Smaller ice crystals, formed during the freezing stage result in a higher specific surface area and so favor moisture desorption during secondary drying, at the expense of a reduction in the rate of ice sublimation (during primary drying) owing to the higher dry layer resistance.

Of final note is that any devitrification of the amorphous phase to the crystalline form will inevitably free up previously bound water, which can lower the glass transition of the remaining amorphous phase, and therefore the collapse temperature, thereby increasing the risk of product collapse. Such changes can also have a deleterious impact on the product in terms of stability of the active drug substance because of an increase in the activity of the residual water phase.

1.11 Process Modeling and Process Analytical Technologies

The determination and control of the ice interface temperature is fundamental to the design of an effective primary drying stage of the lyo cycle.The target is to dry at the highest possible temperature to increase the rate of sublimation from a raised vapor pressure of ice relative to that at the condenser, while ensuring that the interface temperature remains below the collapse temperature.

In the previous section, it was demonstrated that all the invasive product probes (TCs and RTDs) are largely ineffective at measuring the temperature at the ice interface, given their location at the base of the vial and the fact that there is a temperature gradient between the base of the ice and the ice interface. Even if probes were located at the ice interface (which starts at the top of the frozen product), the position of this interface will recede downwards (as the ice sublimes), and the tip of the product probe soon becomes exposed to the gas-filled porous dry layer, the temperature of which is governed only partly by the ice interface temperature. At that point, the measurement becomes highly unreliable. Instead, indirect approaches have been implemented whereby the vapor pressure at the ice interface is predicted from several technical approaches and then converted to temperature using the PT curve of the water phase diagram.

1.11.1 Phase Diagram Pressure–Temperature Curve

Data points along the vapor pressure–temperature profile for ice (see the blue line in Figure 1.10) are provided in various tables within the literature along with predictions from a number of empirical formulae that model real experimental data (e.g. [53, 54]). One of the simplest formula, however, is based semiempirically on the Clausius–Clapeyron equation:

$$\ln(P_i) = c - \frac{L}{R}\left(\frac{1}{T_i}\right) \tag{1.1}$$

where P_i and L are the vapor pressure and latent heat of ice respectively, at an absolute temperature YT_i (K), R is the gas constant (8.31447 J mol^{-1} K^{-1}), and c is a constant that must be determined empirically from the available experimental data. The following forms of the Clausius–Clapeyron expression are taken from Murphy and Koot [55] who used the latent heat of sublimation at the triple point (51,059 J mol^{-1} at 273.15 K) to fit experimental data for the vapor pressure of ice (in Pascal, Pa) across a wide range of temperatures to give

$$P_i = \exp\left(28.9074 - \frac{6143.7}{T_i}\right) \tag{1.2}$$

or

$$\ln(P)_i = 28.9074 - \frac{6143.7}{T_i}. \tag{1.3}$$

Note that the experimentally determined constant 6143.7 is close to the theoretical value obtained from the ratio of the latent heat of sublimation at the triple point to the gas constant ($L/R = 51{,}059/8.31447 = 6141$ K).

If the interface temperature is required from a prediction of the ice vapor pressure, then the following form of the Clausius–Clapeyron relation is used:

$$T_i = \frac{6143.7}{28.9074 - \ln(P)_i} \tag{1.4}$$

where the temperature is given in kelvin (K).

1.11.2 Pressure Rise Test (PRT)

Neumann [56] demonstrated (in a patent published in 1961) that it is possible to predict the ice interface vapor pressure (and hence temperature) on freeze-drying milk from an open container and from small bottles, from the rise in chamber pressure that results if the valve between the drying chamber and condensing chamber is closed for less than 1 minute (preferably 2–10 seconds). When the valve is closed, it effectively stops the flow of water vapor to the condenser, while heat continues to pass from the shelf to the vial, thereby continuing to drive water vapor from the surface of ice and through the dry layer. The result (Figure 1.13a) is a nonlinear rise in the total pressure within the chamber until the chamber becomes saturated, i.e. the chamber pressure now equals the vapor pressure at the ice interface (as opposed to the set chamber pressure that was previously controlled by the vacuum pump and gauge to the point at which the valve was closed). In the process, the pressure drop across the dry layer reduces to zero, and any further drying is, in theory, arrested.

In reality (see Figure 1.13b), the pressure rise profile does not reach a clear plateau, but instead continues to rise, in a linear manner, as a result of a constant flux of gas leaking into the chamber (now that the vacuum pump has been isolated from the chamber). Another factor contributing to the continued rise in pressure is the increase in product temperature that occurs once sublimation is arrested

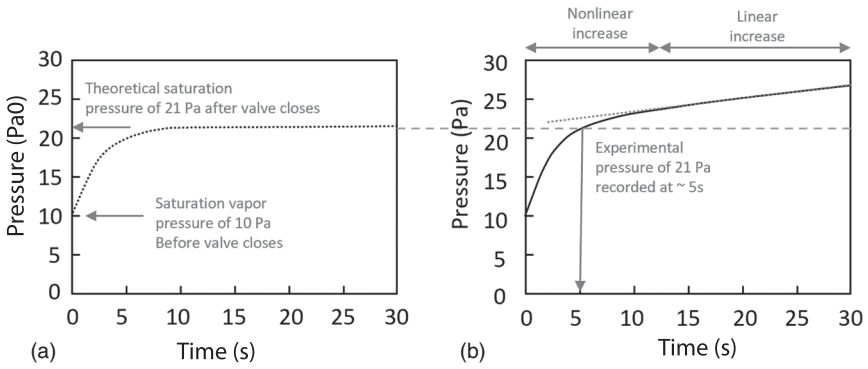

Figure 1.13 Example of pressure rise curve as observed during the primary drying stage of a freeze-drying cycle.

and sublimation-induced self-cooling is lost. The rise in chamber pressure may also increase gas conduction between the shelf and vial, leading to a small increase in the heat transfer coefficient and further warming of the product. Selecting the precise time point at which the saturation pressure should be read from the real experimental pressure rise profile can be calculated using the equation published in Milton et al. [57].

Chapter 5 provides a fuller account of process monitoring methods based on sublimation flow measurement, including pressure rise tests, manometric temperature measurement, pressure rise analysis, dynamic parameter estimation, and related process analytical technologies used during freeze-drying.

1.11.3 Drying Rate Model

Further advances in the prediction of the ice interface pressure became possible with the introduction of the drying rate model proposed by Pikal [58]:

$$\overbrace{\frac{dm}{dt} = \frac{A_{ext} K_v (T_s - T_b)}{L}}^{\text{(A) heat transfer through base of vial}} = \overbrace{\frac{A_{\text{int}} \lambda_i (T_b - T_i)}{h(t) L}}^{\text{(B) heat transfer through frozen layer}} = \overbrace{\frac{A_{\text{int}}}{R_{ps}} (P_i - P_{ch})}^{\text{(C) mass transfer from ice interface to the chamber}}, \qquad (1.5)$$

where dm/dt is the drying rate from ice sublimation. Drying due to desorption of residual (non-crystalline) water is not explicitly included in this primary-drying model, which assumes that sublimation of crystalline ice is the dominant mass-transfer mechanism at the low product temperatures employed. However, as the ice mass diminishes and product temperature rises toward the end of primary drying, desorption contributions may become detectable and can influence the shape of the measured drying-rate or Pirani signal (see Chapter 9). The other parameters in the equation are as follows:

A_{ext}: external cross-sectional area of the base of the vial
A_{int}: internal cross-sectional area of the vial
$h(t)$: height of the ice layer at time t from the onset of ice sublimation
λ_i: thermal conductivity of the frozen layer
K_v: heat transfer coefficient from the surface of the shelf through the base of the vial
T_s: temperature of shelf surface (K)
T_b: temperature at the inside base of the vial
T_i: temperature at the ice interface
P_i: vapor pressure at the ice interface
P_{ch}: vapor pressure in the drying chamber; assumed to equal the total chamber pressure
R_{ps}: resistance to vapor flow through the dry layer and stopper
L: latent heat of sublimation at T_i (e.g. J mol^{-1}) (see Table 1.5 for example values)

The numerator of part A of Eq. (1.5) is the heat transfer from the shelf at a temperature of T_s to the inside base of the vial at a temperature T_b through the vial base.

Table 1.5 Example values for ice vapor pressure and latent heat.

Temperature (K)	Ice vapor pressure (Pa)	Ice latent heat (J mol^{-1})
210	0.70202	51,081
240	27.272	51,139
273.15	611.154	51,059

Source: From Murphy and Koop [55].

This heat transfer is characterized by the effective vial heat transfer coefficient K_v and the external projected surface area of the vial, A_{ext}. Dividing by the latent heat of sublimation, L, the heat transfer is then converted directly to mass transfer, under the assumption that all the heat supplied through the base is used to sublimate the ice, as opposed to increasing the temperature of the ice and its contents.

The numerator of part B of Eq. (1.5) is the heat transfer through the frozen layer from the inside base of the vial to the ice interface at the top of the frozen layer. It is characterized by the thermal conductivity of ice (after correction for the amount of the solids fraction) and the internal cross-sectional area of the vial. Again, by dividing by the latent heat of sublimation, L, the heat transfer is then converted directly to mass transfer.

Part C of Eq. (1.5) is the mass transfer of water vapor from one vial of internal cross-sectional area A_{int} across a resistance to vapor flow associated with the additive resistances of the dried product layer (R_p) and the stopper resistance (R_s), under the driving force of the pressure difference between the vapor pressure at the ice interface (P_i) and the vapor pressure in the chamber (P_{ch}). Under steady-state conditions, the vapor pressure in the chamber is assumed to equal that of the total pressure as measured by the capacitance manometer, which is why the symbol for chamber pressure is used directly. Note that this condition applies, provided that sufficient vapor is being generated by the product and that the flow from the drying chamber to the condensing chamber is not choked by the evolution of too much vapor from the product.

Implementation of this model in the prediction of the ice interface vapor pressure requires a technique for measuring the ice sublimation rate: first, from pure water (to determine the heat transfer coefficient) and then from the drug product solution of interest (to determine the dry layer resistance).

The vial heat transfer coefficient (K_v) is usually determined for vials containing TCs at their base which are placed at selected positions around the dryer, by a gravimetric method involving the preweighing of vials prior to freezing, then after interrupting the cycle once ~25% of the ice has been removed. The drying rate (dm/dt) is then determined from mass lost divided by the duration of the truncated drying period. During this period, the TC measurement of temperature at the base of the vial should remain approximately constant to provide a value for T_b. Note that at some point in time, the ice from around the TC sensor will sublime away, leaving the bead of the sensor exposed, and so the measurement becomes invalid. The other

parameters of part A of the equation, i.e. A_{ext}, T_s, and L, are known, and so it is then possible to determine K_v using the experimentally determined values for dm/dt and T_b. When K_v is known, a drying experiment with the drug product solution of interest is implemented, and again, the drying rate is determined by the gravimetric method.

The one-point gravimetric method, involving the interruption of the cycle and reweighing the vials to determine the mass lost, is somewhat approximate (see Chapter 8, Section 8.3) and relies on an assumption that (i) the dry layer resistance is zero at the start of sublimation and (ii) the dry layer resistance is a linear function of its height. Figure 1.11 demonstrates that these assumptions are not necessarily true for the case when a skin introduces an offset the *y*-axis and any vapor shunts that by-pass the porous dry layer, creates a profile that is curved rather than a straight line. To resolve this issue, a method to determine the drying rate at each time point over the initial part of the primary drying stage is needed. For that purpose, a microbalance technique was developed to profile the rate of drying as a function of time and produce profiles of dry layer resistances. These profiles were then categorized into four types [59].

While the microbalance approach provided valuable insight into the evolution of drying-rate profiles and dry-layer resistance behaviour, it remains an intrusive and laboratory-based technique. In contrast, TVIS, introduced briefly in Section 1.12 and described in greater detail in Chapter 7, provides a noninvasive, *in situ* measurement framework. In Chapter 8, a dedicated ice-sublimation model is developed that enables the instantaneous drying rate, along with the ice-interface and ice-base temperatures, to be determined throughout primary drying. This instantaneous drying rate (derived from the TVIS response) is then introduced into the heat-transfer equations linking the TVIS node to (i) the ice–vapour interface and (ii) the ice base. With an estimate of the thermal conductivity of the frozen matrix, these relationships allow the interface temperature and ice-base temperature to be calculated as functions of time. From these quantities, both the dry-layer mass-transfer resistance and the vial heat-transfer coefficient may be determined as continuous functions of time. This provides a more complete and dynamically resolved characterization of primary drying than is possible with gravimetric or interrupted-cycle methods.

1.11.4 Pressure Rise Modeling

The pressure rise method introduced by Neumann was developed further by Oetjen et al. in 2000. (who patented a model for predicting the ice interface temperature and named the technique the barometric temperature measurement, BTM) [60]. Milton et al. [57] in 1997 and subsequently Tang et al. [61] in 2006 also gave an improved solution with an algorithm that leads to a direct prediction of both the pressure at the sublimation interface (and hence ice interface temperature) and the product dry-layer resistance. These authors adopted the alternative name of manometric temperature measurement (MTM). Pressure rise methods are described in more detail in Chapter 5.

1.11.5 Tunable Diode Laser Adsorption Spectroscopy

The next significant advance was made by Kessler and Gong in 2004 [62] with the first laboratory experiments demonstrating the use of tunable diode laser absorption spectroscopy (TDLAS) for vapor flow monitoring in lyophilization. Then in 2007, Gieseler et al. [63] published the application of TDLAS for the detection of water vapor concentration, gas velocity during freeze-drying process from which the mass flow (i.e. batch drying rate) could then be determined.

Both MTM and TDLAS have been used effectively for modeling the entire sublimation process. These techniques allow for the scale-up (adjustment) of operational parameters to ensure that changes in R_p and K_v from one dryer to another can be accounted to generate the same product temperature profile from one scale to another. In essence, that result is then used to demonstrate the transferability of the process [64–69].

Note that these are large scale batch methods and therefore provide average measurements of the ice interface temperature and dry layer resistance profiles.

1.12 Optical and Spectroscopic PAT Tools

A number of optical spectroscopic methods (including NIR [70–73] and Raman [74–77]) [78–80] and thermal imaging methods using an IR camera [81–84]) have also been developed and applied with some success to batch freeze-drying. However, given the requirement for a line of sight to the test vials, such techniques are somewhat restricted in their full exploitation, as they are unable to characterize any of the vials in the majority core population of the batch. Possibly more importantly, is their application to the "isolated vial" freeze-drying approaches, used in spin freeze-drying and suspended vial freeze-drying, and as an end-product test on 100% of the batch, where lines of sight to each vial are eminently possible. A fuller discussion of spectroscopic PAT methods in freeze-drying, including NIR and Raman spectroscopy, together with associated multivariate data analysis approaches and applications to pharmaceutical freeze-drying, is provided in Chapter 6.

A relatively new method for monitoring the lyophilization cycle in laboratory to pilot scale (developmental) dryers, is TVIS [85, 86]. A distinct advantage of the TVIS approach is that it does not require a line of sight to the test vial, and it is possible to place the TVIS test vials at the core of a small-scale dryer.

TVIS methodology utilizes a pair of electrodes attached directly to the outside of the product container (i.e. the glass vial) with the bottom of the electrode positioned ~ 3 mm from the base. Impedance spectra are generated by the excitation frequency of the applied ac voltage being varied between 10 Hz and 1 MHz (normally with a record of 10 points per decade that are evenly spaced evenly on the log frequency scale). At each discrete frequency, the measured current is referenced back to the applied voltage to generate the magnitude and phase of the impedance of the glass vial and its contents [47], and a spectrum constructed from the individual points. Then, in order to facilitate interpretation, the electrical impedance spectrum

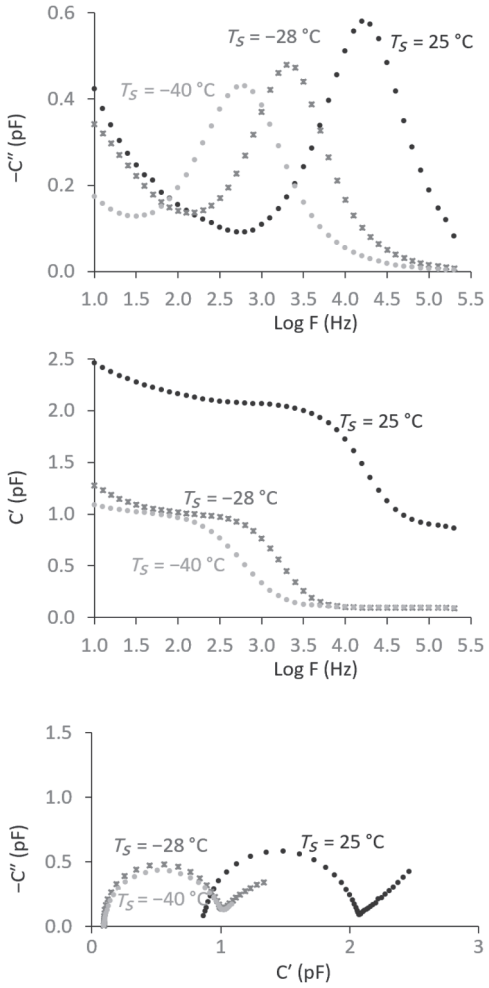

Figure 1.14 Example TVIS spectra for a water-filled vial demonstrating the MW process in the liquid state at +25 °C and the dielectric relaxation of ice in the frozen state at the two temperatures of −28 and −40 °C.

is instead presented in the format of the complex capacitance, i.e. the real and imaginary part capacitances as a function of log frequency (which are known as bode plots) and/or the imaginary part is plotted against the real part (which is known as a complex plane plot or Cole–Cole plot). In this format, a typical relaxation process (for example, the dielectric relaxation of pure ice (Figure 1.14)) is observed as a broad step down in the real part capacitance and a peak in the imaginary capacitance of the bode plots (often referred to as a dielectric loss peak), and a semicircle on the complex plane plot. A charge percolation process will display as a dramatic increase in both the real and imaginary capacitance toward the low-frequency end of the spectrum.

The four main parameters that may be extracted with ease from the complex capacitance spectra are the real part capacitance at low and high frequency, i.e. C' (10 Hz) and C' (100 kHz), and the height and frequency of the peak in the dielectric loss for the ice relaxation, i.e. C''_{PEAK} and F''_{PEAK}.

In the frequency range, 10 Hz–1 MHz, the complex capacitance spectrum of the TVIS vial and contents will display a number of features, depending on the temperature and phase/state of the contents:

i) Relaxation of the Maxwell–Wagner (interfacial polarization) of a water-filled vial.
ii) Dielectric relaxation of ice in frozen water and/or frozen aqueous solution.
iii) Relaxation of the double-layer charging at the surface of the glass.
iv) Percolation of charge through the solids fraction of a frozen solution.
v) Percolation of charge through the hydration surface of the solids fraction once ice has sublimed.
vi) Percolation of charge through the glass wall of the vial.

The TVIS technique is therefore uniquely sensitive to the properties of both the ice fraction and the solids fraction. Applications therefore span the freezing stage (to determine the ice nucleation temperature and ice solidification time [87]—see Figure 1.15) through the annealing stage (to assess devitrification [88], phase separation [89], and Ostwald ripening [90] phenomenon), the primary drying stage, to determine ice and sublimation rates [87] (from which vial heat transfer coefficients [91], and dry layer resistances [87] are calculated) and the ice sublimation end point [92] and finally to the last stage of the process, namely, secondary drying, where it has been shown to characterize the properties of water in nearly dry proteins [93].

Chapters 7–9 provide a more detailed account of through-vial impedance spectroscopy (TVIS) and its application as a process analytical technology for

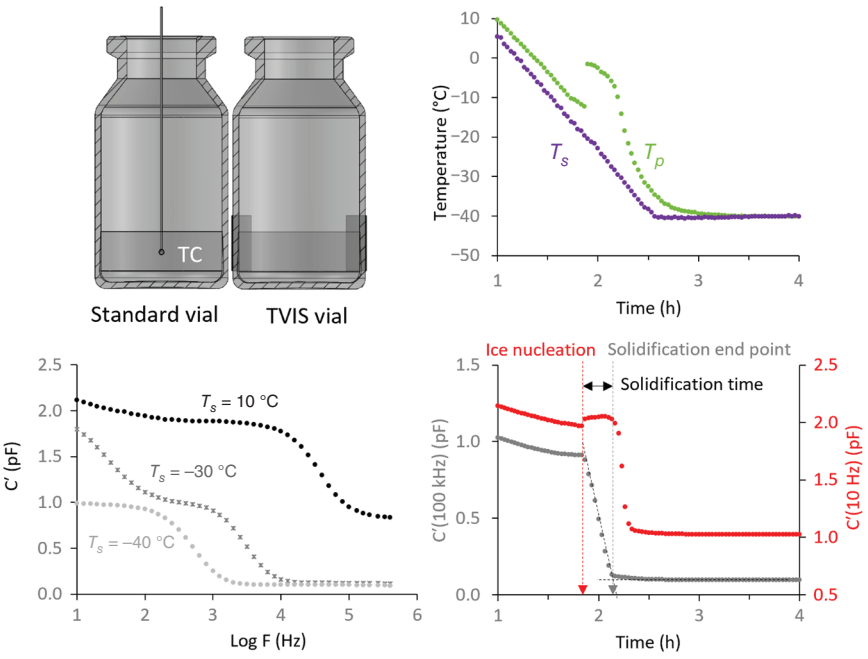

Figure 1.15 Application of TVIS parameters to determine the ice solidification time.

freeze-drying. Chapter 7 introduces the instrumentation, operating principles, electrical modelling, and dielectric basis of TVIS, together with its integration into pharmaceutical freeze-dryers. Chapter 8 then describes the application of TVIS to the characterization and modelling of ice sublimation during primary drying, including the determination of sublimation rates, ice-interface temperatures, heat-transfer coefficients, and dry-layer resistance parameters. Finally, Chapter 9 examines the multiplexing of TVIS with Pirani pressure profiles and related PAT methods for qualitative monitoring of primary drying and prediction of the batch sublimation endpoint.

References

1 Fissore, D., Pisano, R., and Barresi, A.A. (2019). The freeze-drying of pharmaceutical products: introduction and basic concepts. In: *Freeze Drying of Pharmaceutical Products* (ed. D. Fissore, R. Pisano, and A.A. Barresi), 1–10. Boca Raton: CRC Press. https://doi.org/10.1201/9780429022074.

2 Ward, K.R. and Matejtschuk, P. (2019). *Lyophilization of Pharmaceuticals and Biologicals: New Technologies and Approaches*. New York: Humana Press. https://doi.org/10.1007/978-1-4939-8928-7.

3 DiFranco, N. Lyophilization of pharmaceuticals: an overview. https://lubrizolcdmo.com/blog/lyophilization-of-pharmaceuticals-an-overview/ (accessed July, 2025).

4 Gervasi, V., Dall Agnol, R., Cullen, S. et al. (2018). Parenteral protein formulations: an overview of approved products within the European Union. *European Journal of Pharmaceutics and Biopharmaceutics* 131: 8–24. https://doi.org/10.1016/j.ejpb.2018.07.011.

5 Yusoff, Z. (2018). Investing in the future of freeze-drying for biologic drugs. https://www.scrum-net.co.jp/application/files/1617/5552/0647/White_Paper_ControLyo_investing-in-the-future-of-freeze-drying-for-biologic-drugs.pdf (accessed July, 2025).

6 Snyder, M. (2017). Lyophilization: the basics. https://www.drugdiscoverytrends.com/lyophilization-the-basics/ (accessed July, 2025).

7 Kis, Z. (2022). Stability modelling of mRNA vaccine quality based on temperature monitoring throughout the distribution chain. *Pharmaceutics* 14 (2): 430–445. https://doi.org/10.3390/pharmaceutics14020430.

8 Sharma, A., Khamar, D., Cullen, S. et al. (2021). Innovative drying technologies for biopharmaceuticals. *International Journal of Pharmaceutics* 609: 121115. https://doi.org/10.1016/j.ijpharm.2021.121115.

9 Nova Laboratories Ltd. (2016). A green light for cGMP aseptic spray-drying. https://www.manufacturingchemist.com/news/article_page/A_green_light_for_cGMP_aseptic_spray_drying/114844 (accessed July, 2025).

10 Varshney, D. and Singh, M. (2015). *Lyophilized Biologics and Vaccines: Modality-Based Approaches*. New York: Springer. https://doi.org/10.1007/978-1-4939-2383-0.

11 Badal Tejedor, M., Fransson, J., and Millqvist-Fureby, A. (2020). Freeze-dried cake structural and physical heterogeneity in relation to freeze-drying cycle parameters. *International Journal of Pharmaceutics* 590: 119891. https://doi.org/10.1016/j.ijpharm.2020.119891.

12 ICH Harmonized Tripartite Guideline. (2009). Pharmaceutical development Q8 (R2). https://database.ich.org/sites/default/files/Q8%28R2%29%20Guideline.pdf (accessed July, 2025).

13 Jameel, F., Hershenson, S., Khan, M.A., and Martin-Moe, S. (2015). *Quality by Design for Biopharmaceutical Drug Product Development*. New York: Springer. https://doi.org/10.1007/978-1-4939-2316-8.

14 World Health Organization (2015). WHO Expert Committee on Biological Standardization. Sixty-fifth report. *World Health Organization Technical Report Series* 993: 1–262.

15 U.S. Food & Drug Administration (2014). Lyophilization of parenteral (7/93) – Guide to inspections of lyophilization of parenteral (7/93). https://www.fda.gov/inspections-compliance-enforcement-and-criminal-investigations/inspection-guides/lyophilization-parenteral-793 (accessed July, 2025).

16 Seifert, I. and Friess, W. (2019). Established and novel excipients for freeze-drying of proteins. In: *Freeze Drying of Pharmaceutical Products* (ed. D. Fissore, R. Pisano, and A.A. Barresi), 33–52. Boca Raton: CRC Press. https://doi.org/10.1201/9780429022074.

17 Shalaev, E.Y., Wang, W., and Gatlin, L.A. (2008). Rational choice of excipients for use in lyophilized formulations. In: *Protein Formulation and Delivery* (ed. E.J. McNally and J.E. Hastedt), 197–218. New York: Informa Healthcare.

18 Medi, M.B., Chintala, R., and Bhambhani, A. (2014). Excipient selection in biologics and vaccines formulation development. https://www.europeanpharmaceuticalreview.com/article/24136/excipient-selection-biologics-vaccines-formulation-development/ (accessed July, 2025).

19 Challener, C.A. (2017). For lyophilization, excipients really do matter. *BioPharm International* 30 (1): 32–35.

20 Baheti, A., Kumar, L., and Bansal, A.K. (2010). Excipients used in lyophilization of small molecules. *Journal of Excipients and Food Chemicals* 1 (1): 41–54.

21 Manning, M.C., Chou, D.K., Murphy, B.M. et al. (2010). Stability of protein pharmaceuticals: an update. *Pharmaceutical Research* 27: 544–575. https://doi.org/10.1007/s11095-009-0045-6.

22 Janssen Biotech. SYLVANT (siltuximab) [package insert]. https://www.accessdata.fda.gov/drugsatfda_docs/label/2014/125496s000lbl.pdf (accessed July, 2025).

23 Akers, M.J. (2010). *Sterile Drug Products. Formulation, Packaging and Manufacturing*, 138–168. London: Informa Healthcare. https://doi.org/10.3109/9781420020564.

24 Rao, V.A., Kim, J.J., Patel, D.S. et al. (2020). A comprehensive scientific survey of excipients used in currently marketed, therapeutic biological drug products. *Pharmaceutical Research* 37: 1–13. https://doi.org/10.1007/s11095-020-02919-4.

25 Mehmood, Y. and Farooq, U. (2015). Excipients use in parenteral and lyophilized formulation development. *Open Journal of Physiology and Pharmacology* 3 (3): 19–27. https://doi.org/10.1080/03639045.2018.1483392.

26 Powell, M.F., Nguyen, T., and Baloian, L. (1998). Compendium of excipients for parenteral formulations. *PDA Journal of Pharmaceutical Science and Technology* 52 (5): 238–311.

27 Gómez, G., Pikal, M.J., and Rodríguez-Hornedo, N. (2001). Effect of initial buffer composition on pH changes during far-from-equilibrium freezing of sodium phosphate buffer solutions. *Pharmaceutical Research* 18: 90–97. https://doi.org/10.1023/A:1011082911917.

28 Chi, E.I. (2016). Excipients used in biotechnology products. In: *Pharmaceutical Excipients* (ed. O.M.J. Koo), 145–198. Hoboken: Wiley.

29 Pramanick, S., Singodia, D., Chandel, C.V. Excipient selection in parenteral formulation development. https://www.academia.edu/4320620/Excipient_Selection_In_Parenteral_Formulation_Development (accessed July, 2025).

30 Wang, D.Q. (2010). Formulation characterization. In: *Freeze-Drying/Lyophilization of Pharmaceuticals and Biological Products* (ed. L. Rey). Boca Raton: CRC Press. https://doi.org/10.3109/9781439825761.

31 Bjelošević, M., Pobirk, A.Z., Planinšek, O., and Grabnar, P.A. (2020). Excipients in freeze-dried biopharmaceuticals: contributions toward formulation stability and lyophilisation cycle optimisation. *International Journal of Pharmaceutics* 576: 119029. https://doi.org/10.1016/j.ijpharm.2020.119029.

32 Wang, W. (2000). Lyophilization and development of solid protein pharmaceuticals. *International Journal of Pharmaceutics* 203 (1–2): 1–60. https://doi.org/10.1016/S0378-5173(00)00423-3.

33 Oetjen, G.W. and Haseley, P. (2004). *Freeze-Drying*, 2e. Weinheim: Wiley-VHC.

34 Smith G. Simplified Schematic of a Freeze-Dryer. De Montfort University, 2023. https://doi.org/10.21253/DMU.22082879 (accessed July, 2025).

35 Jennings, T.A. (2008). *Lyophilization: Introduction and Basic Principles*. Boca Raton, FL: CRC Press. https://doi.org/10.1201/b14424.

36 Nail, S., Tchessalov, S., Shalaev, E. et al. (2017). Recommended best practices for process monitoring instrumentation in pharmaceutical freeze drying - 2017. *AAPS PharmSciTech* 18: 2379–2393. https://doi.org/10.1208/s12249-017-0733-1.

37 Bhatnagar, B. and Tchessalov, S. (2020). Advances in freeze drying of biologics and future challenges and opportunities. In: *Drying Technologies for Biotechnology and Pharmaceutical Applications* (ed. S. Ohtake, K. Izutsu, and D. Lechuga-Ballestreros), 139–177. Weinheim: Wiley-VCH.

38 Schneid, S. and Gieseler, H. (2008). Evaluation of a new wireless temperature remote interrogation system (TEMPRIS) to measure product temperature during freeze drying. *AAPS PharmSciTech* 9: 729–739. https://doi.org/10.1208/s12249-008-9099-8.

39 Smith, G. (2023). *Freeze-Drying (Lyophilisation) Cycle Recipe*. De Montfort University. https://doi.org/10.21253/DMU.22082882 (accessed July, 2025).

40 Searles, J.A. (2010). Freezing and annealing phenomena. In: *Freeze-Drying/Lyophilization of Pharmaceuticals and Biological Products* (ed. L. Rey), 425–440. Boca Raton: CRC Press. https://doi.org/10.3109/9781439825761.

41 Smith, G. (2023). *Example Freezing Cycle*. De Montfort University. https://doi.org/10.21253/DMU.22082897 (accessed July, 2025).

42 Geidobler, R. and Winter, G. (2013). Controlled ice nucleation in the field of freeze-drying: fundamentals and technology review. *European Journal of Pharmaceutics and Biopharmaceutics* 85 (2): 214–222. https://doi.org/10.1016/j.ejpb.2013.04.014.

43 Gieseler, H. (2012). Controlled Nucleation in Freeze-Drying. https://www.europeanpharmaceuticalreview.com/article/15427/controlled-nucleation-in-freeze-drying/ (accessed July, 2025).

44 Lacey, A.A., Price, D.M., and Reading, M. (2006). Theory and practice of modulated temperature differential scanning calorimetry. In: *Modulated Temperature Differential Scanning Calorimetry* (ed. M. Reading and D.J. Hourston), 1–81. Netherlands, Dordrecht: Springer. https://doi.org/10.1007/1-4020-3750-3.

45 Reading, M., Elliott, D., and Hill, V.L. (1993). A new approach to the calorimetric investigation of physical and chemical transitions. *Journal of Thermal Analysis* 40: 949–955. https://doi.org/10.1007/BF02546854.

46 Blaine, R.L. and Thomas, L.C.Optimization of the freeze drying process using Modulated Differential Scanning Calorimetry®. https://www.tainstruments.com/pdf/literature/TA354%20Optimization%20of%20the%20Free%20Drying%20Process%20using%20MDSC.pdf (accessed July, 2025).

47 Smith, G. and Polygalov, E. (2019). Through vial impedance spectroscopy (TVIS): a novel approach to process understanding for freeze-drying cycle development. In: *Lyophilization of Pharmaceuticals and Biologicals* (ed. K.R. Ward and P. Matejtschuk). New York: New Technologies and Approaches. Humana Press 10.1007/978-1-4939-8928-7.

48 Smith, G. (2023). *Phase Diagram of Water Illustrating the Process of Boiling*. De Montfort University, https://doi.org/10.21253/DMU.22082900 (accessed July, 2025).

49 Smith, G. (2023). *Phase Diagram of Ice Demonstrating the Process of Sublimation*. De Montfort University, https://doi.org/10.21253/DMU.22082903 (accessed July, 2025).

50 Smith, G. (2023). *Product Resistance to Vapour Flow*. De Montfort University. https://doi.org/10.21253/DMU.22082930 (accessed July, 2025).

51 Smith, G. and Wijesekara, P. (2023). *Primary drying profile for 15% IgG formulation*. De Montfort University. https://doi.org/10.21253/DMU.22083086 (accessed July, 2025).

52 Tang, X. and Pikal, M.J. (2004). Design of Freeze-Drying Processes for Pharmaceuticals: Practical Advice. *Pharmaceutical Research* 21 (2), pp. 191–200.

53 Huang, J. (2018). A simple accurate formula for calculating saturation vapor pressure of water and ice. *Journal of Applied Meteorology and Climatology* 57: 1265–1272. https://doi.org/10.1175/JAMC-D-17-0334.1.

54 Wagner, W., Riethmann, T., Feistel, R., and Harvey, A.H. (2011). New equations for the sublimation pressure and melting pressure of H_2O Ice Ih. *Journal of Physical and Chemical Reference Data* 40 (4): 043103. https://doi.org/10.1063/1.3657937.

55 Murphy, P. and Koop, T. (2005). Review of the vapour pressures of ice and supercooled water for atmospheric applications. *Quarterly Journal of the Royal Meteorological Society* 131: 1539–1565. https://doi.org/10.1256/qj.04.94.

56 Neumann, K.H. (1961). Freeze-drying apparatus. U.S. Patent No. 2994132.

57 Milton, N., Pikal, M.J., Roy, M.L., and Nail, S.L. (1997). Evaluation of manometric temperature measurement as a method of monitoring product temperature during lyophilization. *PDA Journal of Pharmaceutical Science and Technology* 51: 7–16.

58 Pikal, M.J., Roy, M.L., and Shah, S. (1984). Mass and heat transfer in vial freeze-drying of pharmaceuticals: role of the vial. *Journal of Pharmaceutical Sciences* 73 (9): 1224–1237. https://doi.org/10.1002/jps.2600730910.

59 Pikal, M.J., Shah, S., Senior, S., and Lang, J.E. (1983). Physical chemistry of freeze-drying: measurement of sublimation rates for frozen aqueous solutions by a microbalance technique. *Journal of Pharmaceutical Sciences* 72 (6): 635–650. https://doi.org/10.1002/jps.2600720614.

60 Oetjen, G.W., Haseley, P., Klutsch, H., and Leineweber, M. (2000). Method for controlling a freeze-drying process. U.S. Patent No. 6163979.

61 Tang, X.C., Nail, S.L., and Pikal, M.J. (2006). Evaluation of manometric temperature measurement, a process analytical technology tool for freeze-drying: Part I, product temperature measurement. *AAPS PharmSciTech* 7 (1): 14. https://doi.org/10.1208/pt070114.

62 Kessler, W.J. and Gong, E. (2019). Tunable diode laser absorption spectroscopy in lyophilization. In: *Lyophilization of Pharmaceuticals and Biologicals. New Technologies and Approaches* (ed. K.R. Ward and P. Matejtschuk), 113–141. New York: Humana Press. https://doi.org/10.1007/978-1-4939-8928-7.

63 Gieseler, H., Kessler, W.J., Finson, M. et al. (2007). Evaluation of tunable diode laser absorption spectroscopy for in-process water vapor mass flux measurements during freeze drying. *Journal of Pharmaceutical Sciences* 96 (7): 1776–1793. https://doi.org/10.1002/jps.20827.

64 Kuu, W.Y., Nail, S.L., and Sacha, G. (2009). Rapid determination of vial heat transfer parameters using tunable diode laser absorption spectroscopy (TDLAS) in response to step-changes in pressure set-point during freeze-drying. *Journal of Pharmaceutical Sciences* 98 (3): 1136–1154. https://doi.org/10.1002/jps.21478.

65 Kuu, W.Y., O'Bryan, K.R., Hardwick, L.M., and Paul, Y.W. (2011). Product mass transfer resistance directly determined during freeze-drying cycle runs using tunable diode laser absorption spectroscopy (TDLAS) and pore diffusion model. *Pharmaceutical Development and Technology* 16 (4): 343–357. https://doi.org/10.3109/10837451003739263.

66 Awotwe Otoo, D., Agarabi, C., and Khan, M.A. (2014). An integrated process analytical technology (PAT) approach to monitoring the effect of supercooling on lyophilization product and process parameters of model monoclonal antibody

formulations. *Journal of Pharmaceutical Sciences* 103 (7): 2042–2052. https://doi.org/10.1002/jps.24005.

67 Rambhatla, S. and Pikal, M.J. (2003). Heat and mass transfer scale-up issues during freeze-drying, I: atypical radiation and the edge vial effect. *AAPS PharmSciTech* 4: E14. https://doi.org/10.1208/pt040214.

68 Rambhatla, S., Ramot, R., Bhugra, C., and Pikal, M.J. (2004). Heat and mass transfer scale-up issues during freeze drying: II. Control and characterization of the degree of supercooling. *AAPS PharmSciTech* 5 (4): 58. https://doi.org/10.1208/pt050458.

69 Gieseler, H., Kramer, T., and Pikal, M.J. (2007). Use of Manometric Temperature Measurement (MTM) and SMARTTM Freeze Dryer technology for development of an optimized freeze-drying cycle. *Journal of Pharmaceutical Sciences* 96 (12): 3402–3418. https://doi.org/10.1002/jps.20982.

70 Kauppinen, A., Toiviainen, M., Lehtonen, M. et al. (2014). Validation of a multipoint near-infrared spectroscopy method for in-line moisture content analysis during freeze-drying. *Journal of Pharmaceutical and Biomedical Analysis* 95: 229–237. https://doi.org/10.1016/j.jpba.2014.03.008.

71 Lin, T.P. and Hsu, C.C. (2002). Determination of residual moisture in lyophilized protein pharmaceuticals using a rapid and non-invasive method: near infrared spectroscopy. *PDA Journal of Pharmaceutical Science and Technology* 56: 196–205.

72 Bobba, S., Zinfollino, N., and Fissore, D. (2021). Application of Near-Infrared Spectroscopy to statistical control in freeze-drying processes. *European Journal of Pharmaceutics and Biopharmaceutics* 168: 26–37. https://doi.org/10.1016/j.ejpb.2021.08.009.

73 Mensink, M.A., Van Bockstal, P., Pieters, S. et al. (2015). In-line near infrared spectroscopy during freeze-drying as a tool to measure efficiency of hydrogen bond formation between protein and sugar, predictive of protein storage stability. *International Journal of Pharmaceutics* 496 (2): 792–800. https://doi.org/10.1016/j.ijpharm.2015.11.030.

74 Sarraguça, M.C., De Beer, T., Vervaet, C. et al. (2010). A batch modelling approach to monitor a freeze-drying process using in-line Raman spectroscopy. *Talanta* 83 (1): 130–138. https://doi.org/10.1016/j.talanta.2010.08.051.

75 Romero-Torres, S., Wikström, H., Grant, E.R., and Taylor, L.S. (2007). Monitoring of mannitol phase behavior during freeze-drying using non-invasive Raman spectroscopy. *PDA Journal of Pharmaceutical Science and Technology* 61: 131–145.

76 de Waard, H., De Beer, T., Hinrichs, W.L.J. et al. (2010). Controlled crystallization of the lipophilic drug fenofibrate during freeze-drying: elucidation of the mechanism by in-line Raman spectroscopy. *The AAPS Journal* 12: 569–575. https://doi.org/10.1208/s12248-010-9215-z.

77 Tsubaki, S., Matsuzawa, T., Fujii, S. et al. (2019). In situ Raman monitoring of dielectric-heating-enhanced freeze-drying under different electromagnetic wave frequencies. *RSC Advances* 9: 91–95. https://doi.org/10.1039/C9RA00981G.

78 Preskar, M., Korasa, K., Vrbanec, T. et al. (2021). Applicability of Raman and near-infrared spectroscopy in the monitoring of freeze-drying injectable ibuprofen. *Drug Development and Industrial Pharmacy* 47 (5): 758–769. https://doi.org/10.1080/03639045.2021.1934864.

79 De Beer, T., Burggraeve, A., Fonteyne, M. et al. (2011). Near infrared and Raman spectroscopy for the in-process monitoring of pharmaceutical production processes. *International Journal of Pharmaceutics* 417 (1-2): 32–47. https://doi.org/10.1016/j.ijpharm.2010.12.012.

80 De Beer, T.R.M., Vercruysse, P., Burggraeve, A. et al. (2009). In-line and real-time process monitoring of a freeze drying process using Raman and NIR spectroscopy as complementary process analytical technology (PAT) tools. *Journal of Pharmaceutical Sciences* 98 (9): 3430–3446. https://doi.org/10.1002/jps.21633.

81 Lietta, E., Colucci, D., Distefano, G., and Fissore, D. (2019). On the use of infrared thermography for monitoring a vial freeze-drying process. *Journal of Pharmaceutical Sciences* 108: 391–398. https://doi.org/10.1016/j.xphs.2018.07.025.

82 Harguindeguy, M., Stratta, L., Fissore, D., and Pisano, R. (2021). Investigation of the freezing phenomenon in vials using an infrared camera. *Pharmaceutics* 13: 1664. https://doi.org/10.3390/pharmaceutics13101664.

83 Harguindeguy, M. and Fissore, D. (2021). Temperature/end point monitoring and modelling of a batch freeze-drying process using an infrared camera. *European Journal of Pharmaceutics and Biopharmaceutics* 158: 113–122. https://doi.org/10.1016/j.ejpb.2020.10.023.

84 Harguindeguy, M. and Fissore, D. (2021). Micro Freeze-Dryer and Infrared-based PAT: novel tools for primary drying design space determination of freeze-drying processes. *Pharmaceutical Research* 38: 707–719. https://doi.org/10.1007/s11095-021-03023-x.

85 Smith, G., Polygalov, E., and Page, T. (2011). A method for monitoring and/or controlling process parameters of a lyophilization process. UK patent, GB2480299A.

86 Smith, G., Polygalov, E., Arshad, M.S. et al. (2013). An impedance-based process analytical technology for monitoring the lyophilisation process. *International Journal of Pharmaceutics* 449 (1-2): 72–83. https://doi.org/10.1016/j.ijpharm.2013.03.060.

87 Jeeraruangrattana, Y., Smith, G., Polygalov, E., and Ermolina, I. (2020). Determination of ice interface temperature, sublimation rate and the dried product resistance, and its application in the assessment of microcollapse using through-vial impedance spectroscopy. *European Journal of Pharmaceutics and Biopharmaceutics* 152: 144–163. https://doi.org/10.1016/j.ejpb.2020.04.015.

88 Smith, G. (2022). What's the point in the end-point? A determination of the true sublimation endpoint by through-vial impedance spectroscopy. https://doi.org/10.21253/DMU.19625946.v1 (accessed July, 2025).

89 Arshad, S, Smith, G, Polygalov, E, et al. (2013) In situ characterization of phase separation in PVP dextran solutions using impedance spectroscopy. AAPS Conference 2013, San Diego, USA. https://doi.org/10.13140/2.1.4818.4327.

90 Smith, G., Arshad, M.A., Polygalov, E., and Ermolina, I. (2014). Through-vial impedance spectroscopy of the mechanisms of annealing in the freeze-drying of maltodextrin: the impact of annealing hold time and temperature on the primary drying rate. *Journal of Pharmaceutical Sciences* 103 (6): 1799–1810. https://doi.org/10.1002/jps.23982.

91 Smith, G., Jeeraruangrattana, Y., and Ermolina, I. (2018). The application of dual-electrode through vial impedance spectroscopy for the determination of ice interface temperatures, primary drying rate and vial heat transfer coefficient in lyophilization process development. *European Journal of Pharmaceutics and Biopharmaceutics* 130: 224–235. https://doi.org/10.1016/j.ejpb.2018.05.019.

92 Pandya, B., Smith, G., Ermolina, I., and Polygalov, E. (2021). Observations on the changing shape of the ice mass and the determination of the sublimation end point in freeze-drying: an application for through-vial impedance spectroscopy (TVIS). *Pharmaceutics* 13 (11): 1835–1851. https://doi.org/10.3390/pharmaceutics13111835.

93 Suherman, P.M., Taylor, P.M., and Smith, G. (2002). Development of a remote electrode system for monitoring the water content of materials inside a glass vial. *Pharmaceutical Research* 19: 337–344. https://doi.org/10.1023/A:1014455304527.